International Journal of Hydrogen Energy 130 (2025) 213–229

Contents lists available at ScienceDirect

International Journal of Hydrogen Energy

journal homepage: www.elsevier.com/locate/he

Effect of process parameters on properties of $Mn_{1.5}CuFe_{0.5}O_4$ spinel oxide coatings deposited by spray pyrolysis method

Maryam Mehdizade [a,*], Federico Smeacetto [b], Michał Winiarski [c], Sebastian Molin [a]

[a] Advanced Materials Center, Faculty of Electronics, Telecommunications and Informatics, Gdansk University of Technology, Gdansk, Poland
[b] Department of Applied Science and Technology, Polytechnic di Torino, Italy
[c] Applied Physics and Mathematics and Advanced Materials Center, Gdansk University of Technology, Gdansk, Poland

ARTICLE INFO

Handling Editor: Søren Juhl Andreasen

Keywords:
Solid oxide cells
Metallic interconnects
Spray pyrolysis
Fe modified Mn–Cu spinel materials
Electrical conductivity

ABSTRACT

One of the critical issues in the lifetime of metallic interconnects is related to their high oxidation rate and Cr diffusion, which negatively affect their performance. In the present study, a novel Fe modified Mn–Cu spinel oxide with the chemical composition of $Mn_{1.5}CuFe_{0.5}O_4$ as protective coating was deposited on the surface of Crofer 22 APU and alumina by the spray pyrolysis method. The effects of different deposition conditions including deposition temperature, spraying speed, and volume of precursor on the properties of deposited spinel coatings were investigated. Scanning electron microscopy characterizations showed that the deposited layer was uniform and non-cracked at the deposition temperature of 400 °C. However, at temperatures of 300 °*C* and lower, the deposited layers became non-uniform and cracked. Additionally, spraying with speeds of 10 ml/h and lower resulted in uniform and non-cracked coatings, and a higher spraying speed of 15 ml/h caused a nonuniform and cracked layer. Atomic force microscopy measurements proposed that the value of R_a was reduced by increasing the deposition temperature and reducing the spraying speed. X-ray diffraction characterization showed that deposition temperature has affected the phase structure of deposited spinel oxides on both substrates. According to electrical conductivity measurements, deposited layers at higher deposition temperatures with lower spraying speeds showed higher electrical conductivity and lower activation energy. Decreasing the deposition temperature reduced the electrical conductivity of the spinel oxide coatings.

1. Introduction

Due to climate change, there is a crucial need to expand technical technologies for clean and renewable energy production and diminish the evolution of greenhouse gases. One of the interesting solutions is green hydrogen technology, which has attracted the attention of scientists in recent years. Solid oxide cells (SOCs) with an efficient capability of green hydrogen production are one of the main technologies for the clean energy market [1–3].

One of the solid oxide cell's limitations is related to degradation of ferritic stainless-steel metallic interconnects during their performance of connecting near cells. The degradation of metallic interconnects directly affects the growth of oxide scales, reduces electrical conductivity, and correspondingly, results in a remarkable decrease in the efficiency of SOCs [4–8]. The critical solution to suppress Cr_2O_3 formation is the deposition of protective ceramic coatings on the surface of metallic interconnects. With their complex structure, thermal stability, and high electrical conductivity, spinel oxide materials are good candidates for protective coatings [1,2,7–12]. Spinel oxides with the general formula of $(AB)_3O_4$ are widely used as protective coatings for metallic interconnects. The structure of spinel coatings consists of A and B cations, which are divalent, trivalent or quadrivalent, located in octahedral and tetrahedral sites and oxygen anions placed on the face-centered cubic lattice sites. $(AB)_3O_4$ spinel protective coatings play an essential role in preventing volatile Cr diffusion to the surface and the formation of Cr_2O_3, which is known as chromium poisoning [2,3,11–13].

Different kinds of spinel oxide materials such as Mn-Co [10,14–16], Mn-Cu [14,17–21], Co-Ni [22–24], Mn-Ni [25], Cu-Fe [26], Ni-Fe [27] and so on are studied by researchers. For example, Geng et al. [26] reported that applied $CuFe_2O_4$ spinel layer significantly limited Cr migration and decreased oxidation rate and area specific resistance. New classes of spinel oxide protective coatings, such as Mn–Cu–Fe spinel oxides, need more investigation to understand their properties and performance in the real SOC device [7,19,28,29]. For example, Acharya

* Corresponding author.
E-mail address: Maryam.mehdizade@pg.edu.pl (M. Mehdizade).

https://doi.org/10.1016/j.ijhydene.2025.04.355
Received 12 March 2025; Received in revised form 17 April 2025; Accepted 19 April 2025

et al. [20] studied the effect of Mn_3O_4 and $CuMn_2O_4$ spinel oxide coatings on oxidation resistance of SUS430 metallic interconnects. They reported that both coatings have good electrical conductivity, and Mn_2CuO_4 spinel oxide coating showed higher area-specific resistance than Mn_3O_4 spinel oxide coating. Ranjbar-Nouri et al. [18] applied Cu–Mn spinel oxide on the ISI-430 ferritic stainless-steel by pulse electrodeposition method to reduce cathode poisoning and oxide growth on the surface of metallic interconnects. Their findings showed that $CuMn_2O_4$ spinel layer effectively controlled Cr diffusion.

Additionally, doping of rare earth elements or transition metals such as Cu [19,20,23,30,31], Fe [22,24,30,32], Ce [31,33,34], Y [35,36], La [35], Gd [36], Ti [37], Nb [37], is proposed as an effective method for further improvement of properties of spinel oxide materials like expansion coefficient, electrical conductivity, oxidation resistance, thermal and chemical stability [7,13,29]. For example, Mazur et al. [17] prepared Ni or Fe doped $Cu_{1.3}Mn_{1.7}O_4$ spinel oxide materials with wet chemistry and solid-state reaction methods. Their results suggested that electrical conductivity further increased by doping higher amounts of Ni. For Ni doped samples, $CuMnNi_{0.1}$ and $CuMnNi_{0.3}$, the reported value of electrical conductivity at 800 °*C*, were 128 and 150 S/cm. At the same time, higher amounts of Fe reduced electrical conductivity. For Fe doped samples, $CuMnFe_{0.1}$ and $CuMnFe_{0.3}$, the reported values of electrical conductivity at 800 °*C*, were 140 and 106 S/cm, respectively. Ignaczak et al. [38] compared the properties of Mn_2CoO_4 coating with Fe doped $Mn_{2-x}CuFe_xO_4$ (x = 0, 0.1, 0.3) spinel oxide coatings. Their findings proposed that Fe-doped Mn_2CuO_4 spinel materials showed significantly higher electrical conductivity compared to Mn_2CoO_4 spinel material at 800 °C. Spinel materials with lower amounts of Fe and a higher ratio of Cu/Mn, because of a higher concentration of Mn^{3+}/Mn^{4+} cations, showed higher electrical conductivity. Additionally, $Mn_{1.7}CuFe_{0.3}O_4$ coating showed the best oxidation resistance after 3000 h. Brylewski et al. [39] found that introducing Cu into the lattice of Mn–Co spinel resulted in a significant increment of electrical conductivity and blockage of outward diffusion of Cr. Their study confirmed that $Cu_{0.3}Mn_{1.1}Co_{1.6}O_4$ spinel oxide coating could be a potential protective-conductive coating on the surface of ferritic steel metallic interconnects.

Furthermore, the production method of protective coatings is an effective factor in the final price and good performance of the coated metallic interconnects. There is a vital need to make it possible to deposit protective coatings with eco-friendly and cost-effective methods. Researchers tried to apply protective coatings with different methods like electrophoretic deposition [16,19,25,28], spin coating [40], spray pyrolysis [41–45], dip coating [46,47], sputtering [5,26,48,49], electrodeposition [18], electroplating [5,22,23,50], powder spray [51] and extra. For example, Hu et al. [52] prepared $Mn_{1.5}Co_{1.5}O_4$ spinel coatings using aerosol spraying method with 5–8 μm thickness. The prepared layer significantly improved oxidation resistance and reduced oxide scale from 4 to 0.75 μm with prevention of Cr diffusion. Sun et al. [53] performed $CuMn_{1.8}O_4$ spinel coatings on flat and mesh metallic interconnects using electrophoretic method. They reported that the coating layer was a combination of Mn_3O_4 and cubic spinel phase at room temperature, and pure cubic spinel phase between 750 and 850 °*C*. The coated interconnects act as an effective Cr getter, resulting in prevention of Cr poisoning of cathode.

Spray pyrolysis as a simple, cost-effective, and reproducible method could be used for large-scale production of coatings on any kind of substrate for different applications [54–56]. Spray pyrolysis is a liquid-based deposition method that results in complete surface coverage through a sequential deposition of atomized droplets splashing on the heated substrate. After random coverage of atomized droplets on the whole surface area, uniform coating layer formation starts and the thickness of the layer increases. Different deposition parameters such as deposition temperature, spraying speed, chemical composition of precursor, and volume of precursor influence the final properties and performance of spinel oxide coatings [54,56–58].

The most important features of a successful deposition of protective coatings by wet chemistry processing methods like spray pyrolysis are to achieve a dense, uniform and defect-free coating, directly affecting the electrical conductivity and oxidation resistance of the metallic interconnects. This purpose is complex because of a need to manage the pyrolysis reactions and obtain equilibrium between spraying, evaporation of organic components and the densification process to form a solid film on the substrate [59–61]. The deposited spinel oxide coatings with wet chemistry methods such as spray pyrolysis could be denser than those with other methods, using powder of the spinel oxide materials [43,45,56,58,60,62–64]. For example, Rupp et al. [59] reported that spray pyrolysis could effectively produce dense, defect-free and amorphous ceria thin films. Simons et al. [60] deposited ceria ceramic thin films by spray pyrolysis method and reported that the spray pyrolysis parameters affected the crack-formation and uniformity of the coating. Ryll et al. [58] deposited defect- and crack-free lanthanum nickelate thin films using the spray pyrolysis, promoting electrical conductivity and area specific resistance. Kamecki et al. [55] proposed that spray pyrolysis method is an effective method for the deposition of thin (Mn, Co, Fe, Ni, Cr)$_3O_4$ spinel oxide coatings with homogenous elemental distribution and defect-free microstructure.

In the present study, Fe modified Mn–Cu spinel oxide material with chemical composition of $Mn_{1.5}CuFe_{0.5}O_4$ is deposited on the surface of Crofer 22 APU and alumina with spray pyrolysis as a simple and effective method. The main objective of this research is to focus on the effects of spray pyrolysis parameters, including deposition temperature, spraying speed, volume of the precursor and distance from the spraying center, on the properties of the deposited spinel oxide coatings. For this purpose, effects of spraying parameters on deposition yield, microstructure, roughness, phase structure and electrical conductivity of $Mn_{1.5}CuFe_{0.5}O_4$ spinel oxide coatings as a new class of protective coating are investigated.

2. Experimental procedures

2.1. Materials

In the present study, $Mn_{1.5}CuFe_{0.5}O_4$ spinel oxide materials were deposited as protective coatings on the surface of Crofer 22 APU ferritic stainless-steel (FSS) metallic interconnect and alumina. Firstly, aqueous solutions of $Mn(NO_3)_2.4H_2O$ (Sigma Adrich, purity ≥97 %), $Cu(NO_3)_2.H_2O$ (Sigma Adrich, purity ≥99.99 %) and $Fe(NO_3)_3.9H_2O$ (Sigma Adrich, purity ≥99.99 %) were prepared at room temperature. Precursor by cations ratios of Mn:Cu:Fe = 3:2:1 by addition of tetra ethylene glycol (4 EG) (Sigma Aldrich, 99 % purity) as organic component was prepared using magnetics stirring at room temperature. The total concentration of cations (total metal ions) in the prepared precursor was 0.1 M (corresponding spinel concentration of 0.0667 M).

Crofer 22 APU sheets (batch number 104754334, VDM-Metals, Verdohl, Germany) with chemical composition reported in Table 1, and dimensions of 20 × 20 × 0.3 mm^3, and commercial alumina sheets with dimensions of 10 × 20 × 1 mm^3 were used as substrates for deposition of $Mn_{1.5}CuFe_{0.5}O_4$ spinel oxide material.

Table 1
Chemical composition of used Crofer 22 APU as substrate in this research.

Element	Fe	Cr	Mn	La	Ti	Si	Al
Weight percentage (Wt.%)	base	23 %	0.45 %	0.1 %	0.06 %	<0.05 %	<0.05 %
EDS composition (Wt.%)	base	21.86 %	0.69 %	–	–	–	–

2.2. Deposition of coating layer

In order to deposit the $Mn_{1.5}CuFe_{0.5}O_4$ spinel oxide layers, the spray pyrolysis method, which is schematically shown in Fig. 1, was used. First, at room temperature, substrates were ultrasonically cleaned for 10 min in a mixture of acetone + isopropanol to remove contaminations. Samples were located on the heating plate and heated to the desired temperature, and subsequently the precursor was sprayed using the Paasche VL airbrush. Both Crofer 22 APU and alumina substrates were coated at different deposition temperatures, including 250, 300, 350 and 400 °C, with a spraying speed of 7.5 ml/h. Additionally, both substrates were coated at constant deposition temperature of 400 °*C* with different spraying speeds including 5, 7.5, 10 and 15 ml/h. Finally, in constant conditions including the deposition temperature of 400 °*C* with the spraying speed of 7.5 ml/h, different volumes of precursor including 20, 40, 80 and 100 ml were sprayed on the surface of both substrates. The precursor was atomized into droplets at an air pressure of 2 bar. The distance between the atomizing nozzle and the heated substrates was 60 cm. Some of the coated samples were sintered at 800 °C for 3 h with heating and cooling rate of 3 °C/min in the static air atmosphere and were compared with the coated samples without the sintering process.

2.3. Characterization

The effectiveness of spray pyrolysis as a simple and productive method for preparation of spinel oxide coatings was evaluated in the terms of deposition yield according to the below equations:

$$\text{Deposition yield } (g/cm^2) = \frac{(m_a - m_b)}{S} \quad (4)$$

In this equation (4), m_a is the weight of substrate after deposition process (g), m_b is the weight of substrate before deposition process (g) and S is the surface area of the sample which is exposed to the sprayed droplets (cm^2). Additionally, the efficiency of the spray pyrolysis process was calculated. The ratio of the total weight of the deposited oxide coatings to the weight of the oxides inside precursor defines the efficiency of the spray pyrolysis method.

Surface and cross sectional of the deposited $Mn_{1.5}CuFe_{0.5}O_4$ spinel oxide coatings after thermal treatment (800 °C for 3 h in the static air atmosphere) were investigated by a scanning electron microscope (SEM), Phenom XL (Thermo Fisher Scientific), equipped with an energy dispersive X-ray spectrometry (EDS) for chemical composition evaluation with an acceleration voltage of 20 kV and a pressure of 10 Pa. For the cross sectional imaging, the samples were embedded in epoxy resin (EpoFix, Struers) and polished to 1 μm finish by the help of an automatic Struers Tegramin-20 machine. A very thin carbon layer was deposited on the cross section of the deposited coatings for better charge transfer and high resolution. A Bruker D2 Phaser second generation (Bruker AXS, Germany) X-ray diffractometer (XRD) with CuKα radiation (λ = 1.5404 Å) and XE-T detector at 40 KV and 30 mA was used to investigate phase structure of the deposited spinel oxide coatings in the as-deposited state and after thermal treatment (800 °*C* for 3 h in the static air atmosphere). The spectra data were collected in a range of 2θ = 10°–70° with a scanning speed of 0.01°/s and accounting time of 2 s for each step. The results were analyzed using the High score plus software. The crystalline size (D) of the prepared cubic spinel oxide coatings can be calculated using the Scherrer formula:

$$D = ((K\lambda))/((\beta \cos \theta)) \quad (5)$$

In this equation, λ is the wavelength of the X-rays, which is 0.15406 nm for Cu-K*α*, K shows the shape factor, which is equal to 0.9, β indicates the FWHM determined from Expert software, and θ is the Bragg diffraction angle.

A Nanosurf easyscan 2 (Nanosurf AG) controller Atomic Force Microscopy (AFM), was used to measure roughness of the coating layers in the contact mode. Obtained data were analyzed using Gwyddion software to calculate average roughness of the deposited coatings. Moreover, the Van Der Pauw method measured electrical conductivity of $Mn_{1.5}CuFe_{0.5}O_4$ spinel oxide coatings. For this purpose, a coated alumina sample with the dimensions of 10 × 20 × 1 mm^3 was contacted at the middle of the sides to platinum wires by silver paste. Platinum wires were connected to an automatic measurement including electrode multiplexer and a Keithley 2400 SourceMeter. Multiplexer applies required changes of electrodes for Van Der Pauw technique [38,41]. The constant current working mode with a current value of 0.1–1 mA based on the resistance value was utilized. Any possible thermovoltage presence was corrected by the system with switching current direction. The electrical conductivity measurement was performed in the temperature

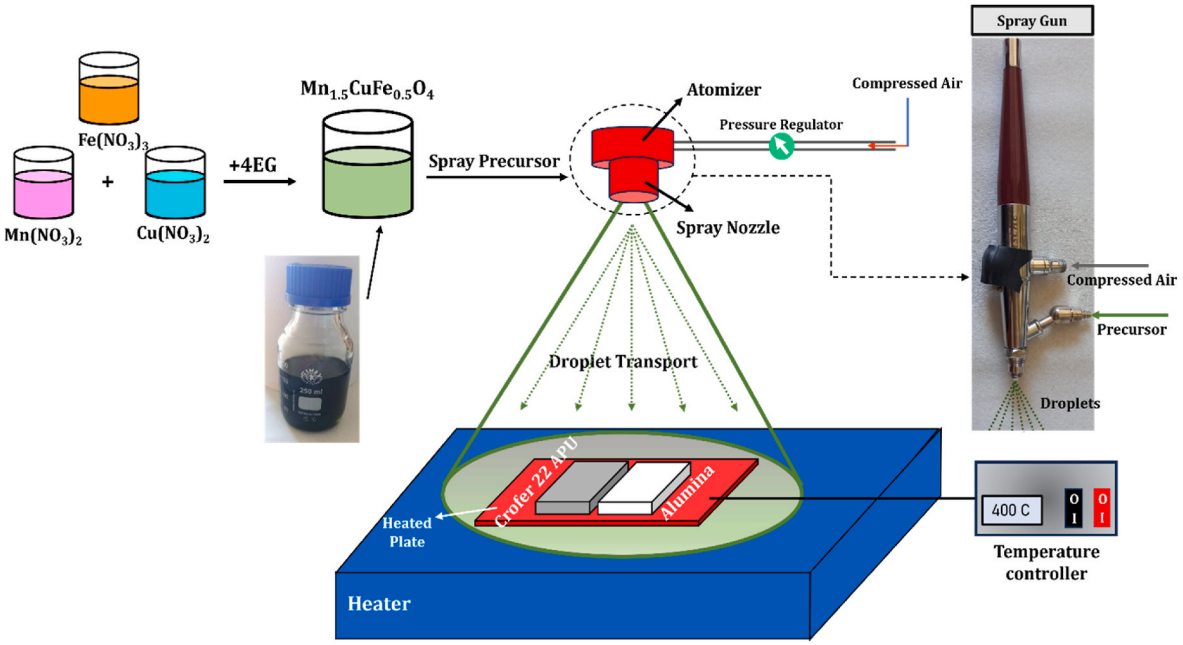

Fig. 1. Schematic illustration of spray pyrolysis method used for preparation of $Mn_{1.5}CuFe_{0.5}O_4$ spinel oxide coatings in this research.

range of 850 °C down to 200 °C with cooling steps of 50 °C and keeping time of 1 h in the static air atmosphere, which is schematically shown in Fig. S1 in the supplementary file. The electrical conductivity of the spinel oxide coatings has an inverse relation with the porosity percentage of the coating layer, according to the Bruggeman asymmetric model equation, which is reported below:

$$\sigma = \frac{\sigma_m}{(1-p)^{\frac{3}{2}}} \quad (6)$$

Where, σ (S cm^{-1}) is the modified electrical conductivity value, σ_m (S cm^{-1}) shows the obtained electrical conductivity value and P is the average percentage of the coating layer, which could be estimated through cross sectional SEM characterization.

3. Results and discussions

3.1. Deposition yield

To improve the oxidation resistance of ferritic stainless-steel interconnects, a thick and uniform protective oxide layer must be provided, and the thickness must be kept below the critical range of crack formation. For this purpose, deposition parameters correlated with pyrolysis reactions, including evaporation of organic components and densification occurring simultaneously during film formation on the substrate, should be controlled.

In this study, spray pyrolysis parameters including deposition temperature, spraying speed, volume of precursor and distance from the center of sprayed precursor, were examined to provide opportunity for deposition of thick, dense, uniform and crack-free Fe modified Mn_2CuO_4 spinel oxide coating. Fig. 2 shows the deposition yield and crack formation of coatings for the deposited spinel oxide coatings at the different deposition conditions on both substrates. As explained in the experimental part, weight changes of the substrate after the deposition process are related to the formation of spinel oxide coatings, which could be considered as the deposition yield of the spray pyrolysis method. Deposition yield could be a function of the temperature of the substrate when droplets reach the surface, spraying speed, volume of precursor, distance from the center of the spraying direction and the kind of substrate.

According to plots, with increasing the volume of the sprayed precursor, the values of deposition yield increase, which could be correlated to higher thickness of the formed coating layers and is in good agreement with SEM results, which will be discussed in detail in the following sections. Most research on spray pyrolysis reports that substrate tem-

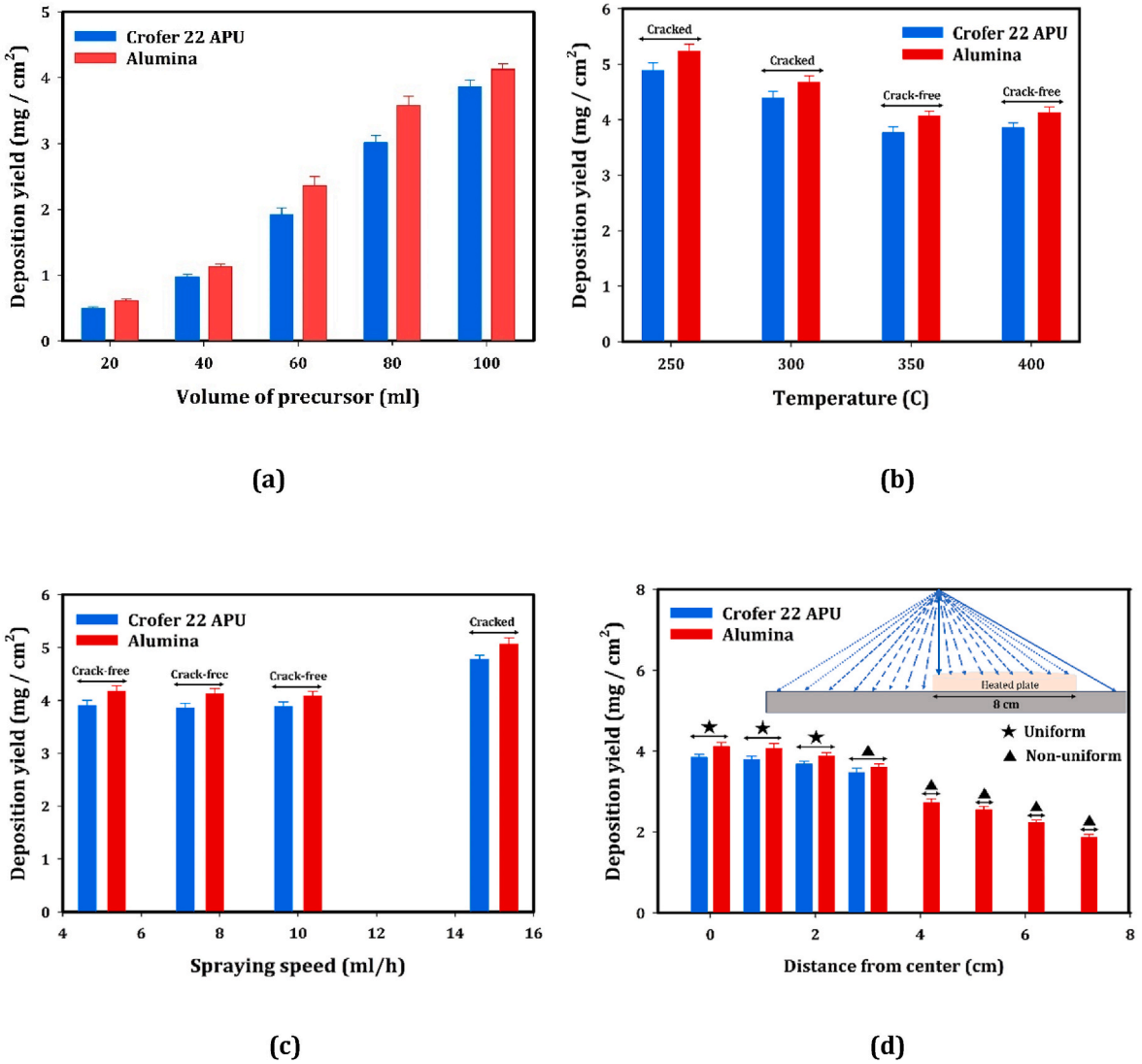

Fig. 2. Deposition yield of prepared spinel oxide coatings by spray pyrolysis method as a function of (a) volume of precursor, (b) deposition temperature, (c) spraying speed, (d) distance of center.

perature during deposition is the most critical parameter [65–67]. According to Fig. 2 (b), at 350 and 400 °*C*, deposition yield is lower compared to 250 and 300 °*C*, and there is a slight difference between them. In spray pyrolysis, the temperature must be high enough for pyrolytic decomposition of organic precursors. This happens when the organic solvent evaporates, and the metal salt crystallizes as it hits the heated surface. Adjusting the temperature during spray pyrolysis helps to control rates of two simultaneous reactions, evaporation and crystallization, which monitor the deposition yield, microstructure, and quality of the densified coating layer [60]. In other words, the kinetics of drying and decomposition of atomized droplets and growing coatings are responsible for forming uniform and crack-free coatings. As a result, the higher deposition yields at temperatures below 300 °*C* are likely related to the residual of solvent. Beckel et al. [67] reported that the ratio of deposition temperature to boiling temperature of solvent is an effective factor in producing uniform and crack-free coatings. Lower ratio of deposition temperature to boiling temperature of solvent could cause lower drying and decomposition kinetics of atomized droplets. At the same time, a higher ratio of deposition temperature to boiling temperature of solvent could lead to fast evaporation and decomposition of atomized droplets. Therefore, this ratio is lower for the deposited coatings at 250 and 300 °C, than those at higher temperatures. So, at lower temperatures, some droplets are still wet when hitting the surface; however, at higher temperatures, most droplets are already dry when touching the substrate's surface. Therefore, the residuals in a growing layer at lower temperatures could lead to different shrinkage and crack formation.

In addition, spraying speed does not significantly affect deposition yield, and with increasing spraying speed from 5 up to 10 ml/h, the deposition yield is slightly decreased. With increasing spraying speed to 15 ml/h, because of lower kinetics of drying and decomposition of atomized droplets, some are still wet when attached to the substrate surface, resulting in residuals. Because of different shrinkage of residuals, cracks could be formed at the deposited coatings with higher spraying speed. Our results propose that the optimized spray pyrolysis conditions for the deposition of Fe modified Mn-Cu spinel oxide layer including temperature and spraying speed are 350–400 °*C* and 5–10 ml/h, respectively.

Furthermore, changes of deposition yield versus distance from center are shown in Fig. 2 (d). According to Fig. 2 (d), the deposition yield significantly decreases in distances more than 3 cm from the center, and the coatings become nonuniform with partial surface coverage. Generally, increasing distance of samples from the center of spraying direction results in partial delivery of atomized droplets on heated substrates and consequently formation of nonuniform coating with random surface coverage. Supplementary results regarding center effect on deposition yield are reported in Fig. S2. Additionally, the efficiency of spray pyrolysis refers to how much of the oxides present inside the precursor is converted into solid oxide coating during the spray pyrolysis process. The efficiency of spray pyrolysis for the Crofer 22 APU and alumina substrates was 10.25 % and 10.9 %, respectively.

3.2. Microstructure

Top-view SEM characterization was used to evaluate the quality of the deposited spinel oxide layers prepared by the spray pyrolysis. Fig. 3 shows the top-view SEM images of the deposited $Mn_{1.5}CuFe_{0.5}O_4$ spinel oxide layers on the surface of Crofer 22 APU and alumina at different deposition temperatures with the same spraying speed (7.5 ml/h) and volume of precursor (100 ml). It is observable that the deposition temperature is one of the critical parameters at the formation of uniform, dense and crack-free coatings on the surface of both substrates (Crofer 22 APU and alumina). At the temperature of 250 °*C*, most parts of surface are covered with microscale cracks and delamination. At this temperature, some organic residue remained on the surface of the floating and different shrinkage resulted in crack formation. Increasing the temperature up to 300 °C remarkably reduces the number and size of cracks, however, some pores and cracks are observable on the surface. By increasing the temperature up to 350 and 400 °C, the deposited spinel coatings showed a uniform and non-cracked microstructure. Additionally, increasing temperature significantly reduces the number of pores in the deposited coatings. The deposited coating at 400 °*C* presented the most dense and uniform microstructure.

Preparing coatings with the exact chemical composition is challenging with wet chemistry methods such as spray pyrolysis. The chemical composition of the deposited coatings was characterized using SEM equipped with an energy dispersive spectroscopy detector (SEM/EDS). To avoid errors in the Fe amount of chemical composition of the deposited spinel oxide coatings, a coated alumina sample at 400 °C with a spraying speed of 7.5 ml/h, was selected for EDS and Map analyses. Also, to provide more reliable results, measurements were performed at five different points, and the average values are reported. According to the elemental analyses results shown in Fig. 4 (a), there is no agglomeration or impurity in the microstructure of the deposited coating and all elements are uniformly distributed throughout the coating. According to Fig. 4(b) and (c), some Cu precipitates are formed on the surface, while no Cu compounds are present throughout the cross section of the coating. The formation of copper oxide may be related to the diffusion of Cu to the surface and its subsequent reaction with oxygen. The measured atomic ratios of Mn to Fe and Cu to Fe are approximately 2.88 ± 0.021 and 2.1 ± 0.01, respectively, which is close to the chemical composition of $Mn_{1.5}CuFe_{0.5}O_4$ spinel oxide. Additionally, to reduce errors in estimating the chemical composition of the deposited coatings, elemental analysis was performed across the cross section of the coating over a larger area. According to the results, the estimated chemical composition of the coating throughout the cross section closely matches our desired composition. There is strong agreement between the average point analyses and the elemental analysis over the larger area. Obtained results show that $Mn_{1.5}CuFe_{0.5}O_4$ spinel oxide layers were successfully produced with spray pyrolysis as a potential method to produce high quality and uniform coatings with different chemical composition on various substrates based on the appropriate chemical composition of precursors.

Furthermore, Fig. 5 demonstrates the top-view SEM images of the deposited $Mn_{1.5}CuFe_{0.5}O_4$ spinel oxide coatings on the surface of Crofer 22 APU and alumina with different spraying speeds at the same deposition temperature. For Crofer 22 APU substrate, at the spraying speed of 5, 7.5 and 10 ml\h, the deposited spinel oxide coatings showed uniform, and non-cracked microstructure. However, by increasing the spraying speed to 10 ml/h, some tiny pores are observable on the surface. However, at the spraying speed of 15 ml/h, there is nonuniform coating covered with cracks and defects. It means that deposition temperatures lower than 350 °*C* and spraying speeds higher than 10 ml/h are not appropriate to control two simultaneous pyrolysis reactions including drying organic components and growth of solid oxide layer for Crofer 22 APU substrate.

In comparison between Crofer 22 APU and alumina substrates, according to Fig. 5 (b), the deposited spinel oxide layers on alumina with different spraying speeds from 5 up to 15 ml/h, show uniform and non-cracked microstructure. There are some tiny pores on the surface of the deposited spinel oxide layers with spraying speeds of 10 and 15 ml/h and their number and size increase with increasing spraying speed.

One of the possible reasons for this difference between deposited spinel oxide layers with spraying speeds of 10 and 15 ml/h on Crofer 22 APU and alumina might be related to higher thermal conductivity of alumina compared to Crofer 22 APU, which are approximately 30–35 and 15 W/mk, respectively. Based on the results, temperature of 400 °*C* and spraying speeds of 7.5 ml/h and lower would be the best conditions for the deposition of spinel oxide coatings on alumina.

Fig. 6 depicts the surface morphology of the deposited $Mn_{1.5}CuFe_{0.5}O_4$ spinel oxide coatings with different volume of the precursor at 400 °*C* with spraying speed of 7.5 ml/h on Crofer 22 APU and alumina. It

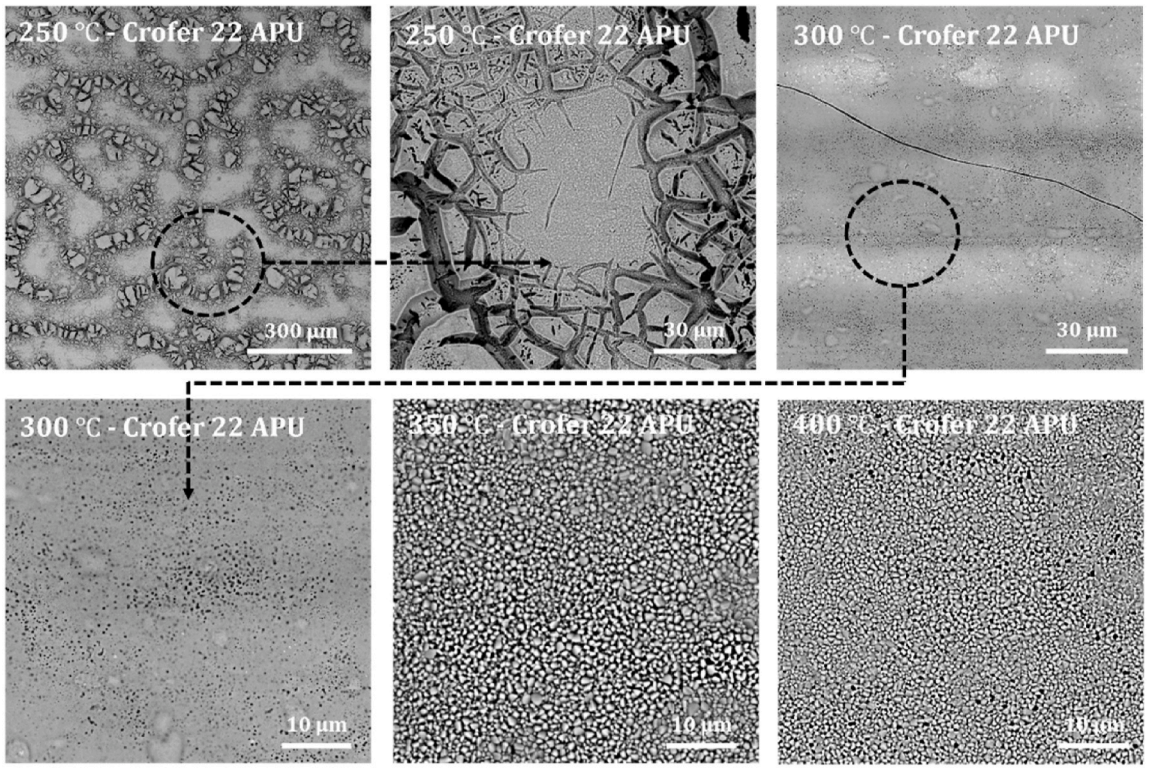

(a)

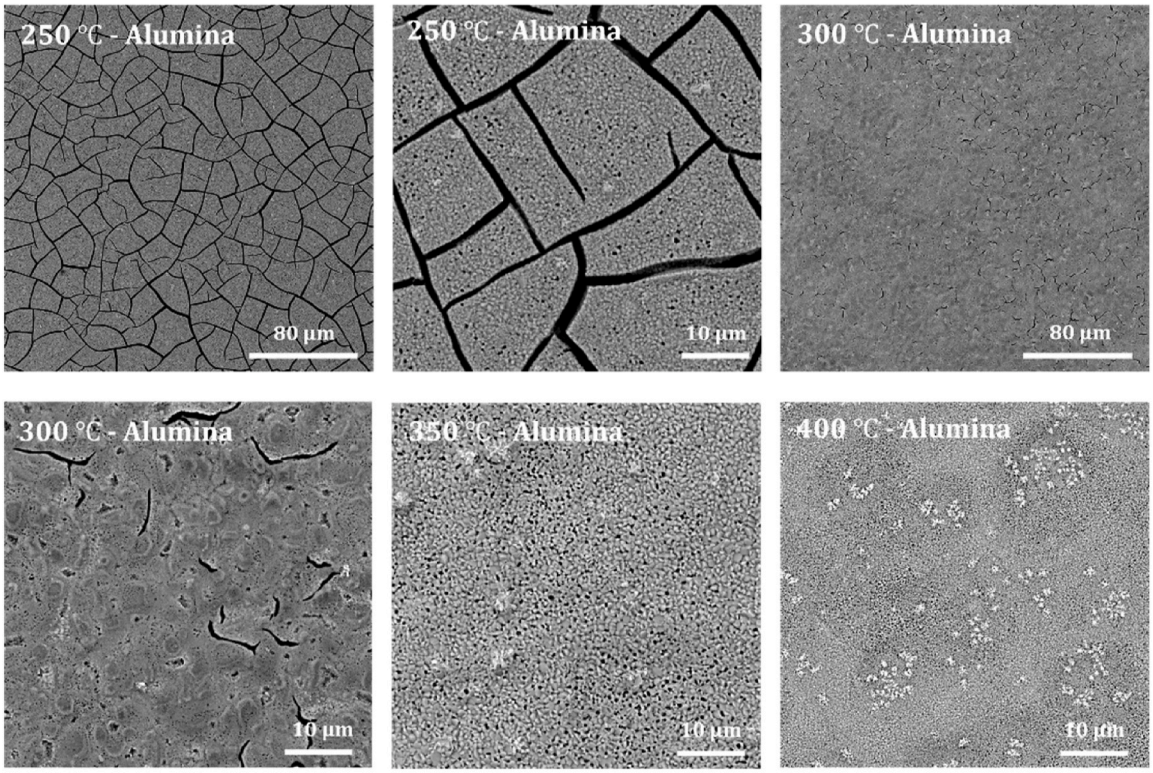

(b)

Fig. 3. The top-view SEM images of the deposited $Mn_{1.5}CuFe_{0.5}O_4$ spinel oxide coatings on: (a) Crofer 22 APU and (b) alumina substrates at different deposition temperatures with 7.5 ml/h spraying speed and 100 ml of precursor.

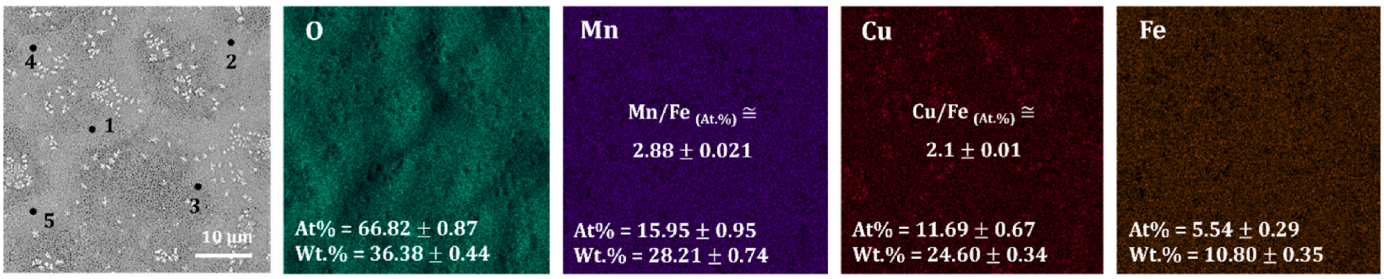

(a)

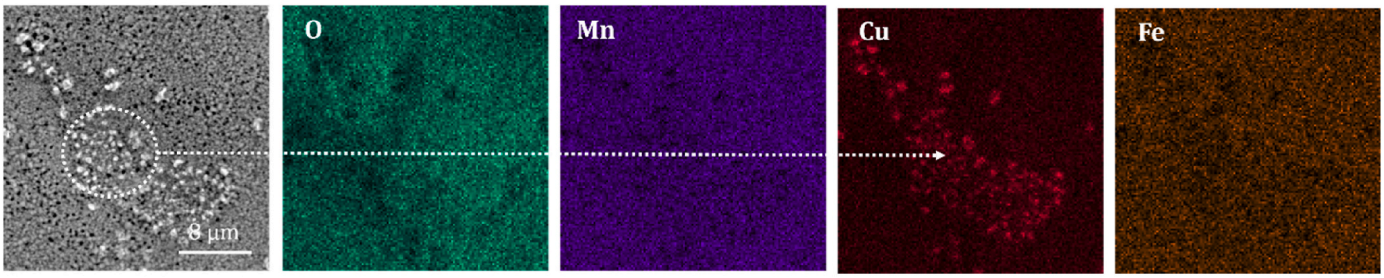

(b)

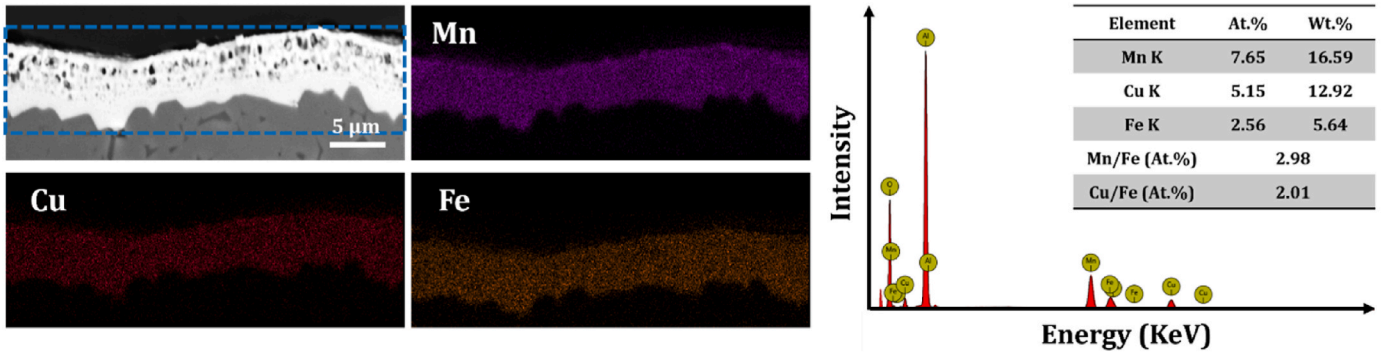

(c)

Fig. 4. (a) Elemental analyses showing the elemental distribution across the surface of the deposited coating and the chemical composition at designated points; (b) high-magnification mapping results showing Cu precipitates on the surface; and (c) elemental analyses showing the elemental distribution and chemical composition across the cross section of the deposited coating (larger area). The coatings were produced at 300 °C (c) and 400 °C (a and b) with a spraying speed of 7.5 ml/h using 100 ml of precursor on an alumina substrate.

is observable that with increasing volume of the precursor there is no significant difference in the microstructure of the deposited coatings on both substrates.

It is needed to find optimized preparation conditions for thick, uniform and non-cracked spinel oxide coatings through the spray pyrolysis method. The thickness and porosity percentage variations of the deposited spinel oxide coatings on both substrates were investigated using cross sectional SEM images and are reported in Fig. 7.

According to Fig. 7 (a), the thickness of the deposited spinel oxide coatings prepared with 100 ml of precursor and spraying speed of 7.5 ml/h, decreases from 7.19 µm to 6.08 µm for Crofer 22 APU substrate and from 7.55 µm to 6.59 µm for alumina substrate, with decreasing temperature from 400 °*C* to 300 °*C*. This behavior is most likely related to the incomplete decomposition of precursor droplets because of insufficient thermal energy at lower temperatures, which results in less solid material being deposited onto the substrate. In this case, droplets may sit on the surface without reacting, and evaporating during coating process or during sintering process, without decomposing and contributing to the formation spinel oxide coating. Additionally, film growth is related to the nucleation and adhesion of the decomposed droplets. At lower temperature, reaction kinetics and diffusion processes may be slowed down, which is more likely to result in the formation of a less dense and thinner coating layer [68]. The sprayed droplets of the precursor splash on the uniform surface of the coating and by growth of spinel oxide layers, droplet to droplet helps to increase the thickness of the spinel oxide coating. Consequently, with increasing deposition temperature, the porosity percentage of the deposited spinel oxide coatings reduces to approximately 70.1 % and 55.4 % for Crofer 22 APU and alumina substrates, respectively.

Additionally, volume of the precursor is the most critical factor in the thickness variations. As shown, with increasing volume of the precursor from 20 to 100 ml, the thickness of coatings on Crofer 22 APU increases

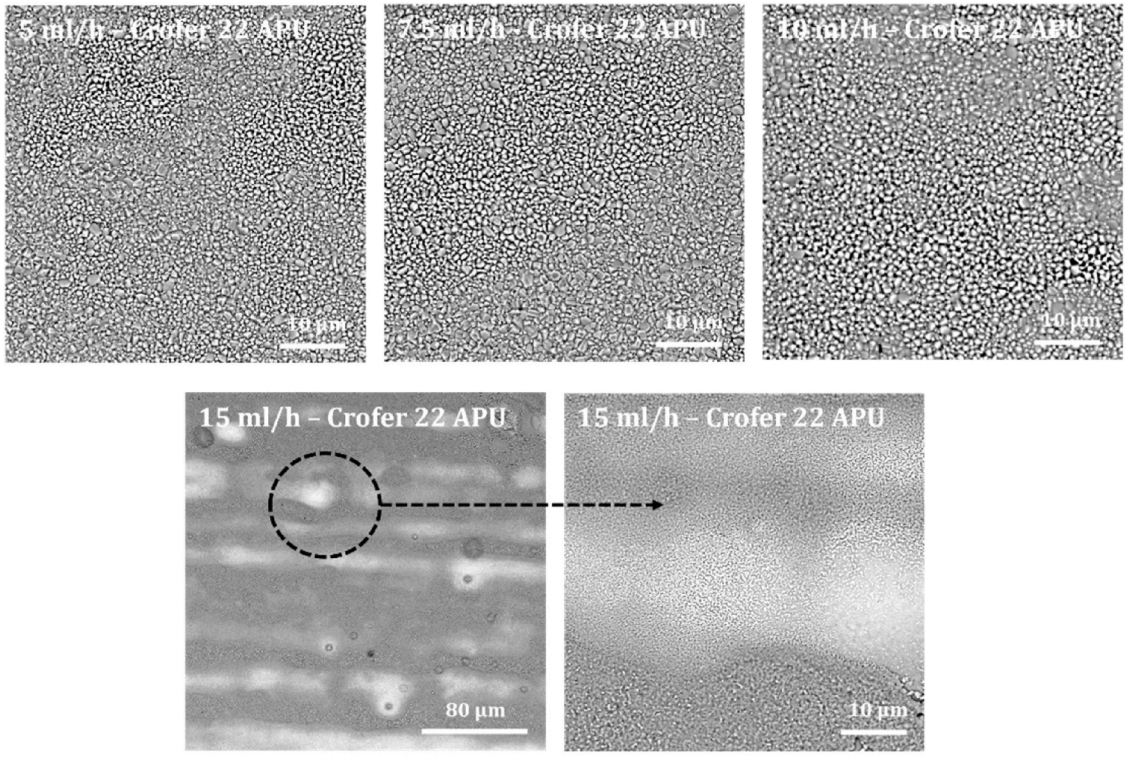

(a)

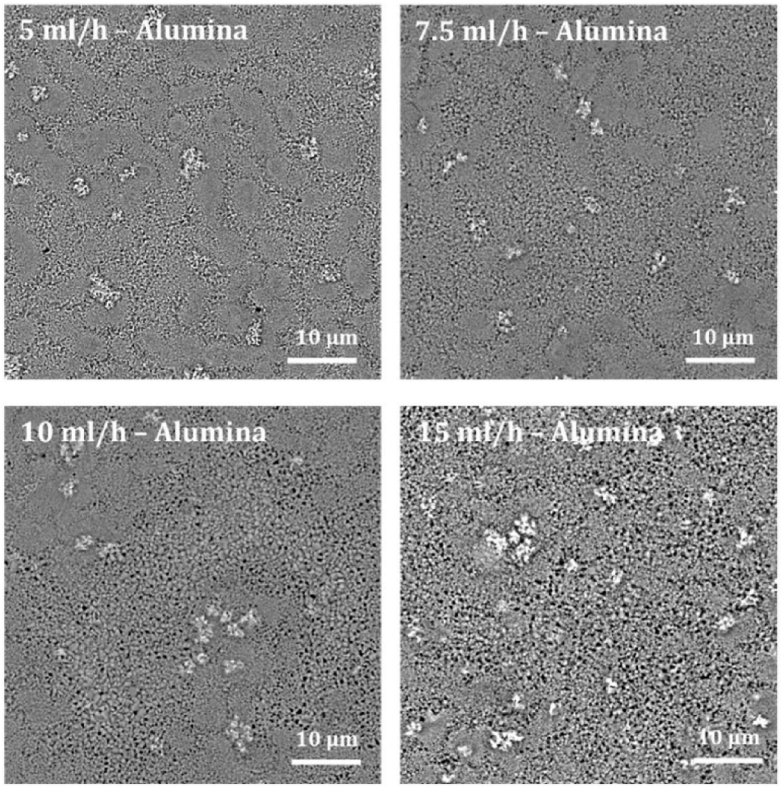

(b)

Fig. 5. The top-view SEM images of the microstructure of deposited $Mn_{1.5}CuFe_{0.5}O_4$ spinel oxide coatings on: (a) Crofer 22 APU and (b) alumina substrates with different spraying speeds at deposition temperature of 400 °*C* and 100 ml of precursor.

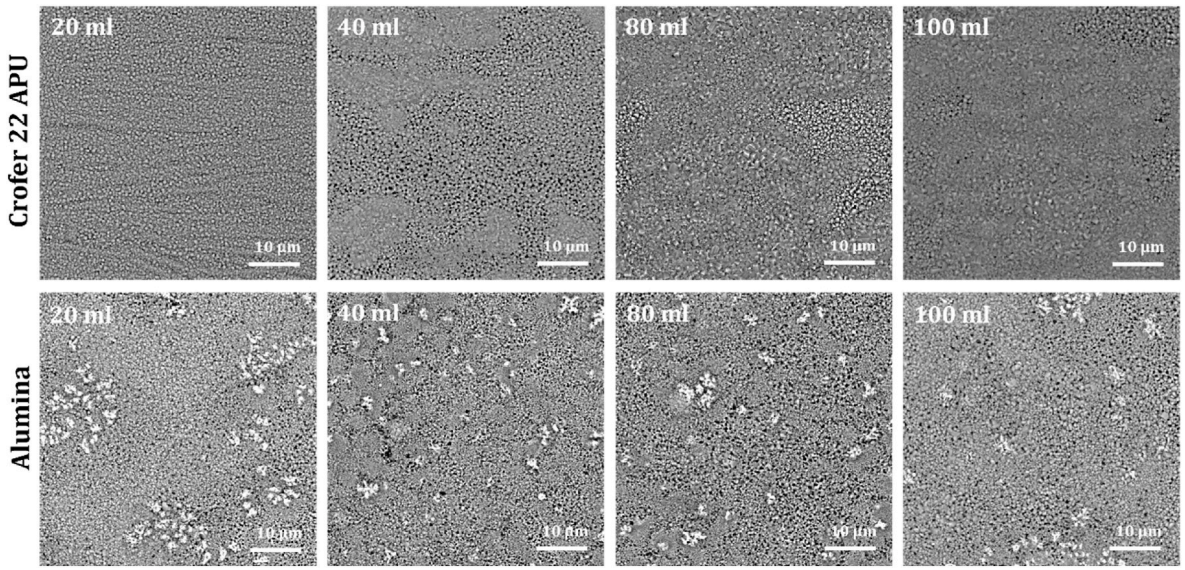

Fig. 6. Top-view SEM images showing microstructure of the deposited $Mn_{1.5}CuFe_{0.5}O_4$ spinel oxide coatings with different volume of the precursors on Crofer 22 APU and alumina.

from 1.66 µm up to 7.19 µm and on alumina from 1.73 µm up to 7.55 µm. With increasing amount of the sprayed and splashed droplets, spinel oxide coating grows layer by layer. It seems, with increasing volume of the precursor, the porosity percentage of the deposited spinel oxide coatings reduces to approximately 36.2 % and 32.3 % for Crofer 22 APU and alumina substrates, respectively. In the beginning of the deposition process, because of random placing of the droplets some small pores could be created. Some of the pores with continuing deposition process (increasing volume of the precursor) eliminate from the upper surface; however, some of them remain and their size increase. So, the porosity percentage of the deposited spinel oxide coatings is intensely influenced with temperature.

Effect of spraying speed on the thickness of the deposited spinel oxide coatings on both substrates is discussed in Fig. S3 in the supplementary file.

Fig. 8 demonstrates the EDS line scan curves for the spinel oxide coatings prepared at 300 and 400 °*C*, after sintering at 800 °*C* for 3 h. The deposited spinel oxide coating at the deposition temperature of 400 °*C*, significantly suppressed Cr diffusion alongside the diffusion zone compared to the deposited spinel oxide coating at the deposition temperature of 300 °C. In fact, the dense structure of the coating and reduced number of the pores and holes are the most important factors in inhibition of Cr diffusion and formation of oxide scale in the interface of the deposited coating and steel substrate. Additionally, different elements are uniformly distributed throughout the thickness of coating.

3.3. Surface topography

The surface topography of the deposited spinel coatings was investigated with AFM measurements, which helps to analyze the physical properties of the prepared spinel oxide layers. Fig. 9 shows AFM images (area of 10 × 10 μm^2) of the deposited spinel coatings at the different temperatures with different spraying speeds after thermal treatment at 800 °*C* for 3 h. Additionally, the values of the calculated average roughness (R_a) for each sample are reported in Table 2. A repeating structure with valleys and hills is detectable in all deposited coatings. According to results, the average roughness of the deposited spinel coatings decreases from 19.93 nm to 12.17 nm, with increasing the deposition temperature from 300 °*C* to 400 °*C*. The AFM image of the prepared spinel coating at 250 °*C* is not reported due to its cracked and nonuniform microstructure. It is more likely correlated to equilibrium between spraying of precursor, evaporation of organic components and deposition of solid spinel oxides on the substrate, which is anticipated to be more stable in the higher temperatures [60]. In prepared coatings at 350 °*C* and 400 °*C*, no microstructural defects like cracks, voids and delamination are observed. Additionally, with increasing spraying speed from 5 ml/h up to 15 ml/h, the value of average roughness is enhanced from 10.04 nm up to 21.65 nm. Because when precursor is sprayed with higher speed, equilibrium between spraying, evaporation and solidification decreases and results in formation of more rough coating layer full of defects (reported in SEM section). Spraying speeds up to 10 ml/h leading to formation uniform coating layer without significant defects on the surface. In conclusion, spraying at low temperature with high spraying speed is not appropriate for deposition of uniform, defect-free and non-cracked spinel coatings on the surface of Crofer 22 APU. Prepared coatings with spraying speed of 15 ml/h at 400 °*C* and with spraying speed of 7.5 ml/h at 300 °*C* and lower, did not show defect-free microstructure, which could be related to lack of stable equilibrium between spraying, evaporation and deposition.

3.4. Phase structure

Fe modified Mn–Cu spinel oxide layers were prepared by the spray pyrolysis method, which is described in detail in the experimental section. To investigate the effect of spray pyrolysis parameters and thermal treatment on the phase structure of spinel oxide coatings, the coated samples at different temperature before and after sintering were characterized by X-ray diffractometry method. Fig. 10 (a) and (b) demonstrate the X-ray diffraction patterns of the deposited coatings at 300 °*C* and 400 °*C* with spraying speeds of 7.5 ml/h on the surface of Crofer 22 APU and alumina substrates before and after sintering at 800 °*C* for 3 h in static air atmosphere.

Regarding Fig. 10 (a), diffraction peaks related to the steel substrate are detectable in both deposited spinel oxide layers at 300 and 400 °*C*, before and after thermal treatment. Additionally, the peaks related to the single phase of $Mn_{2 \pm x}Cu_{1 \pm x}O_4$ spinel oxide with cubic crystal structure and Fd3m space group (PDF No. 00-034-1400) are detectable for both deposited spinel oxide coatings before and after sintering treatment. In its crystal structure, oxygen atoms create a face-centered cubic close-packed lattice and some of the metallic cations occupy the octahedral sites, in contrast, other metallic cations occupy the tetrahedral sites within the lattice. The peaks of cubic spinel for the deposited

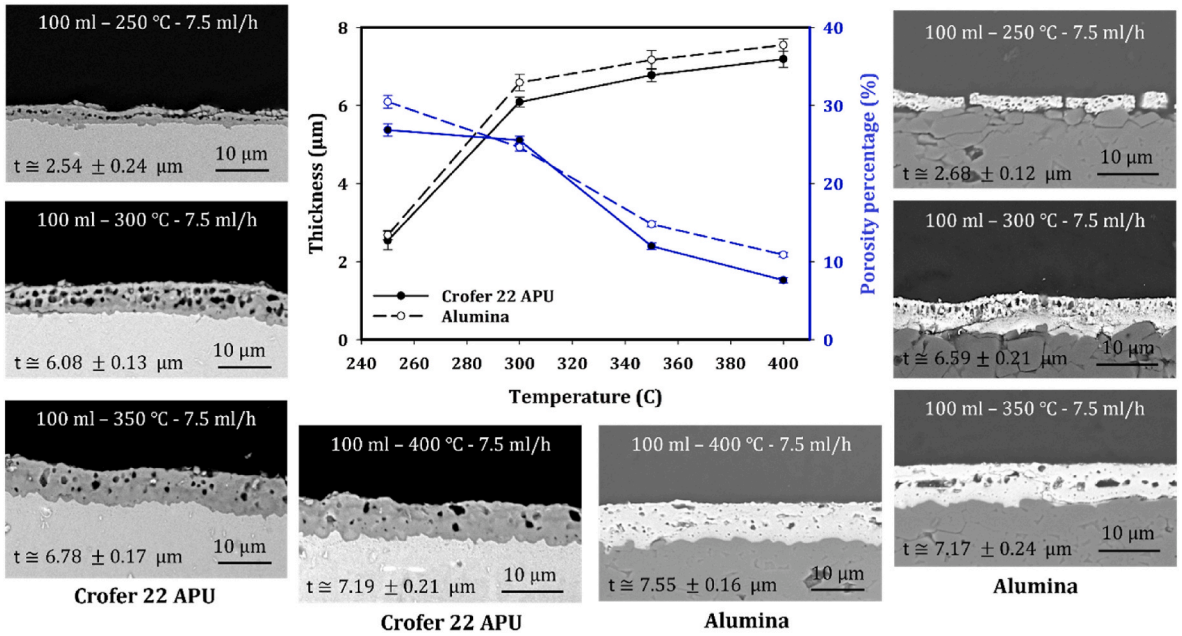

(a)

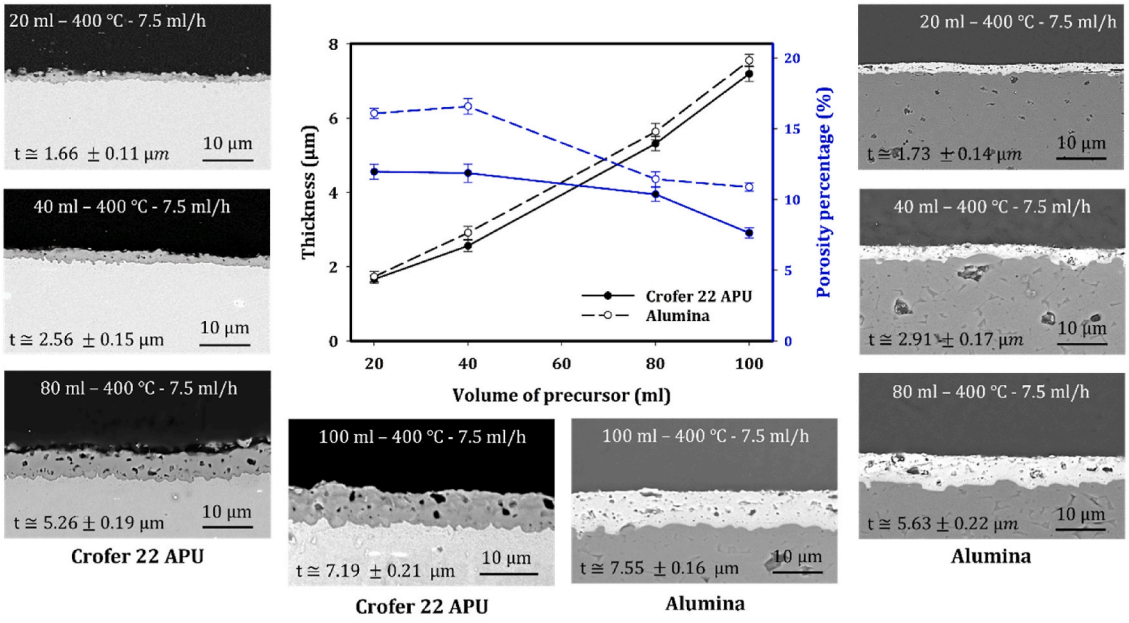

(b)

Fig. 7. Cross sectional SEM view showing (a) the effect of volume of precursor, and (b) effect of deposition temperature on the thickness and porosity percentage of $Mn_{1.5}CuFe_{0.5}O_4$ spinel oxide coatings on Crofer 22 APU and alumina substrates.

spinel oxide coating at 400 °*C* and sintered at 800 °*C*, are slightly shifted to higher values of 2θ compared to that of at 300 °*C*. This diffraction angle shift is likely related to slight crystallization during deposition at higher temperature. Cubic spinel oxide peaks for the deposited coatings, become narrower with increasing deposition temperature and by applying sintering treatment because of slight increase in crystalline size. Narrower peaks show higher crystallinity of cubic spinel structure. In the as-deposited spinel oxide coating at 300 °*C* before sintering thermal treatment, all of the peaks related to cubic spinel oxide are not completely detectable; however, in the as-deposited coating at 400 °*C* before sintering thermal treatment, diffraction peaks located at 2θ (degree) ≅ 18.46, 30.11 and 35.46 are detectable. The mentioned peaks present wider shape and prove slightly crystallization of spinel oxide during deposition process. In other words, the deposited spinel oxide

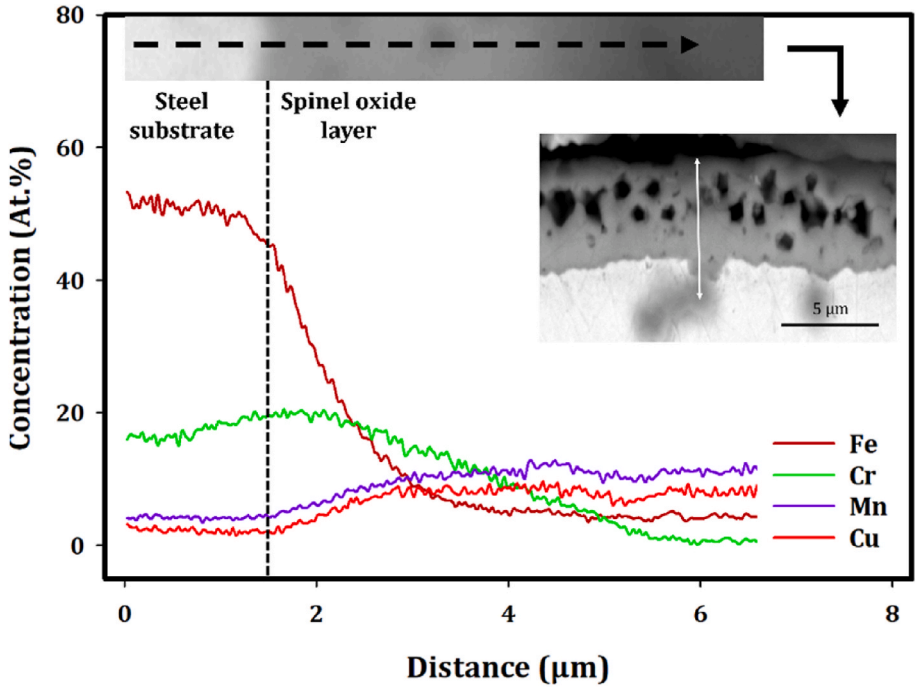

(a)

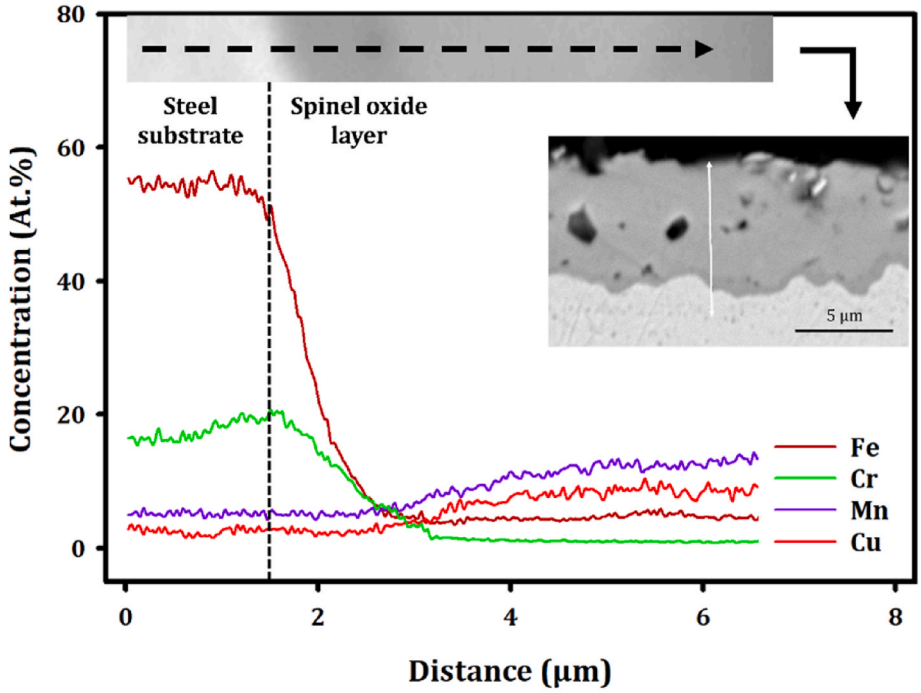

(b)

Fig. 8. The EDS line scan results throughout thickness of the sintered spinel oxide coating prepared at (a) 300 °*C* and (b) 400 °*C*.

coating at 300 °*C* is highly amorphous; however, the deposited spinel oxide coating at 400 °*C* is partially crystallized during deposition process. By comparing XRD pattern of the deposited spinel oxide coatings at 400 °*C* before and after sintering thermal treatment, there is not considerable peak shift, but peaks with the diffraction angle of 42.91 and 62.35 appeared after sintering thermal treatment. Additionally, diffraction peaks correlated to tetragonal spinel oxide with chemical composition of $Mn_{2\pm x}Cu_{1\pm x}O_4$ and *I*41/*amd* group space (PDF No. 01-071-1142) are detectable for the deposited coating at 400 °*C* after sintering treatment. However, the mentioned peaks are not completely detectable for the deposited coating at 300 °*C*. The values of calculated crystalline size of the spinel oxide layers deposited on Crofer 22 APU at

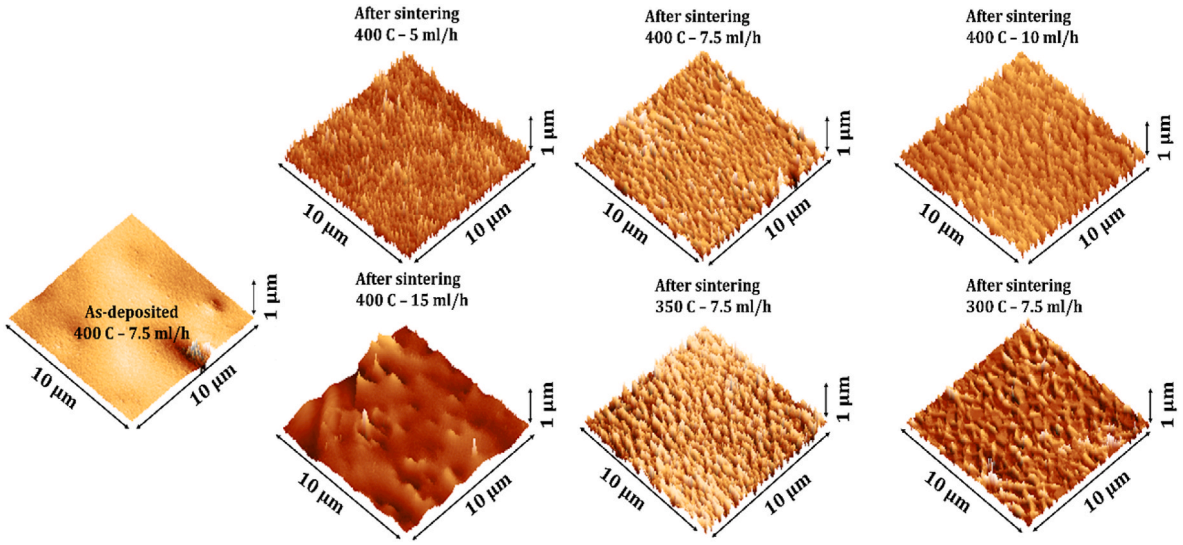

Fig. 9. AFM images in 10 × 10 µm^2 of surface area of the deposited $Mn_{1.5}CuFe_{0.5}O_4$ spinel oxide coatings at temperature of 300, 350 and 400 °*C* with spraying speed of 5, 7.5, 10 and 15 ml/h, before and after sintering at 800 °*C* for 3 h.

Table 2
The values of Ra obtained from AFM measurements for the deposited $Mn_{1.5}CuFe_{0.5}O_4$ spinel oxide at the different temperatures with different spraying speeds before and after sintering.

Deposition temperature (°*C*)	Spraying speed (ml/h)	Sintering	R_a (nm)
400	7.5	×	19.93
	5	✓	10.04
	7.5	✓	12.17
	10	✓	17.49
	15	✓	19.07
350	7.5	✓	16.73
300	7.5	✓	18.56

300 and 400 °C, after the sintering process, is approximately 49.37 and 74.6 nm, respectively. Our results are consistent with the data reported by other researchers [20,38,69].

Furthermore, according to Fig. 10 (b), in the deposited spinel oxide coatings on alumina after and before sintering at 800 °*C* for 3 h, peaks related to the substrate are detectable. Additionally, there are identified peaks related to single phase of $Mn_{2\pm x}Cu_{1\pm x}O_4$ spinel oxide with cubic crystal structure and Fd3m space group (PDF No. 00-034-1400). The diffraction peaks related to this phase are slightly shifted to the lower diffraction angles with increasing deposition temperature from 300 to 400 °*C*, which is likely correlated with a partial crystallization during deposition and slight unit cell size increase. Despite the deposited spinel oxide coatings on Crofer APU 22, the diffraction peaks related to tetragonal spinel oxide coatings are not detectable for the deposited spinel oxide coatings on alumina. The average crystalline size for the deposited spinel oxide layers on alumina at 300 and 400 °C after sintering process calculated by Scherrer formula is approximately 70.45 and 106.93 nm, respectively. In comparison between as deposited and thermally treated spinel coating's XRD pattern, diffraction peaks of spinel oxide at diffraction angles of 2θ (degree) ≅ 30.4, 35.77and 63.22, become visible after sintering treatment due to crystallization of the spinel oxide coating. The mentioned diffraction peaks of spinel oxide become narrower with increasing deposition temperature from 300 up to 400 °*C*, because of a slight increase of crystalline size and partial crystallization during deposition. Furthermore, there are no detectable peaks correlated with Mn or Cu oxides, which means that pure spinel phases are synthesized without presence of precipitation. Our results are in good agreement with other researches [17,38].

Furthermore, according to XRD results of the deposited spinel oxide coatings at 300 and 400 °C before sintering, it seems that formation of spinel oxide phases just starts around 300 °C, which strongly agrees with the literature [70]. As the temperature increases, additional peaks related to spinel phase are revealed. Also, even at 400 °C, the spinel phase is not fully crystallized. After sintering at 800 °C, most of the peaks related to the spinel phases become visible.

3.5. Electrical conductivity

The electrical properties of the deposited spinel oxide coatings were investigated using measurement of the DC electrical transport properties of the sintered coatings in the static air atmosphere at the temperature range of 200–850 °*C* using Van Der Pauw method. Because of steel's conductivity, it is impossible to measure the electrical conductivity of spinel oxide coatings on Crofer 22 APU. Therefore, the deposited oxide spinel on the surface of alumina was selected for electrical conductivity measurements.

Fig. 11 (a) shows the electrical conductivity versus temperature curve. The obtained electrical conductivity data were corrected using estimated porosity percentages of the coating layer by Image J software. Fig. 11 (b) demonstrates the diagram of modified electrical conductivity versus temperature. The measured average porosity percentages for the deposited spinel oxide coatings are shown in Fig. 11 (c). By considering the effect of the porosity of the deposited spinel oxide coatings, the values of the electrical conductivity for all samples are increased.

It is observable that the value of electrical conductivity increases with increasing deposition temperature. The prepared spinel oxide coatings at deposition temperature of 400 °*C* show the higher value of electrical conductivity (σ) because of their denser, uniform, defect-free and non-cracked microstructure. While prepared spinel oxide coatings at lower deposition temperatures present reduced electrical conductivity due to cracks, voids and delimitations in their microstructure. Formation of microstructural defects inside coating results in blocking the movement of charge transfer species and increases the sensitivity of metallic interconnects to corrosion and oxide scale growth. Additionally, with increasing spraying speed due to formation microstructural defects in the spinel oxide coating, the electrical conductivity value slightly reduces. Our findings regarding electrical conductivity values propose that prepared spinel oxide coatings by spray pyrolysis shows acceptable electrical properties to be used as protective coatings for metallic interconnects in real SOC stacks without any disruption in electrical properties.

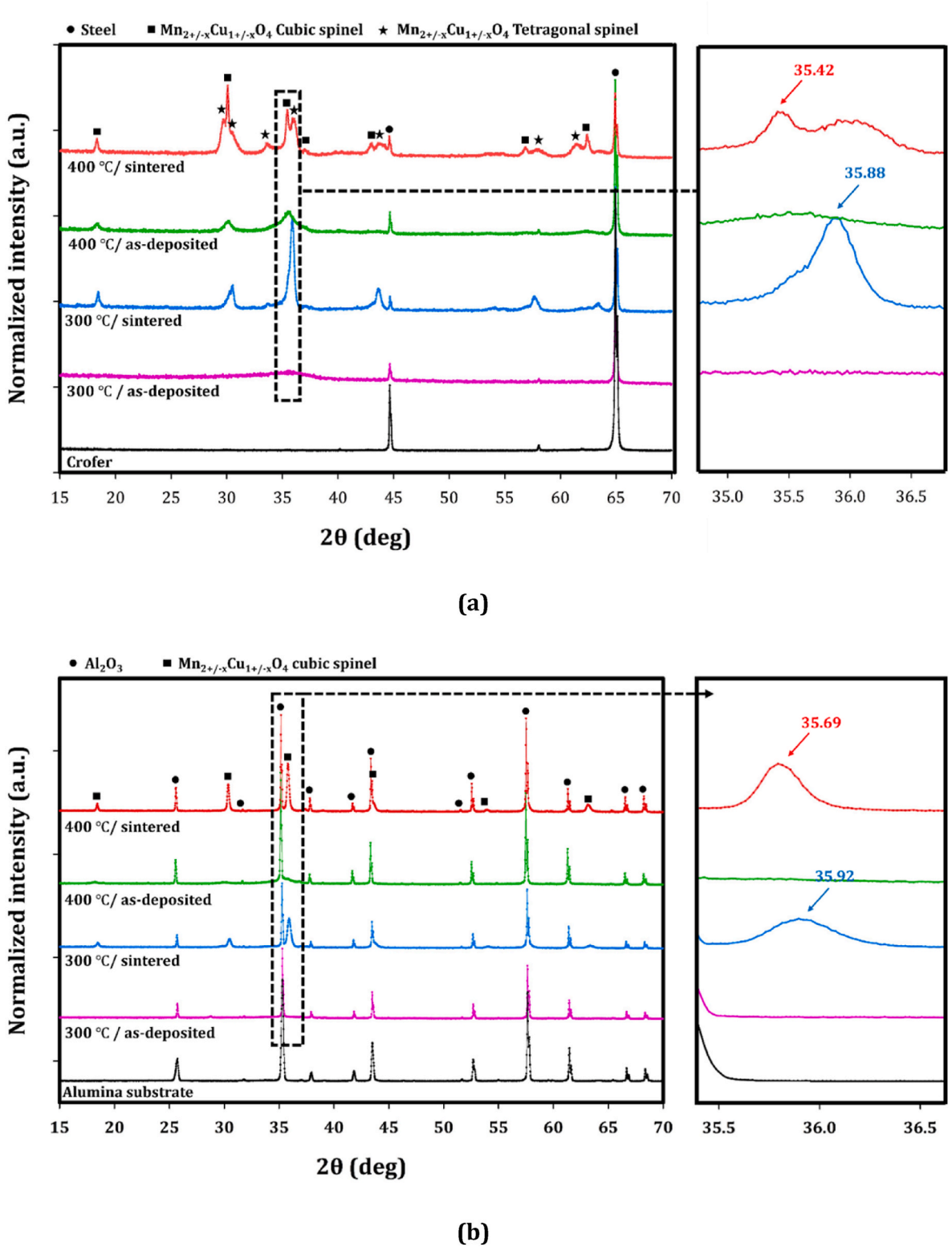

Fig. 10. XRD patterns of deposited $Mn_{1.5}CuFe_{0.5}O_4$ spinel coatings at different temperatures on the surface of (a) Crofer 22 APU and (b) alumina.

Because of multiple valence states inside the lattice of Mn_2CuO_4 spinel oxide materials, they can serve as high temperature conductors. It is known that conduction mechanisms for manganite spinel oxide materials such as Mn_2CuO_4 spinel oxide are based on hopping of charge between octahedral sites. Indeed, hoping charge between $Mn^{3+} \leftrightarrow Mn^{4+}$ exchanging pairs placed in octahedral sites are responsible for promoting the electrical conductivity [71,72]. In the hopping process, charge carrier mobility is a temperature-dependent mechanism and can be conceptualized by activation energy. It is expected that by enhancing thermally activated mobility of charge transfer carriers based on the hopping conduction mechanism, the electrical conductivity will increase. The activation energy for the electrical conductivity variations according to the hopping conduction mechanism can be obtained by Arrhenius relation [73]. Fig. 11 (d) depicts Arrhenius diagrams for the

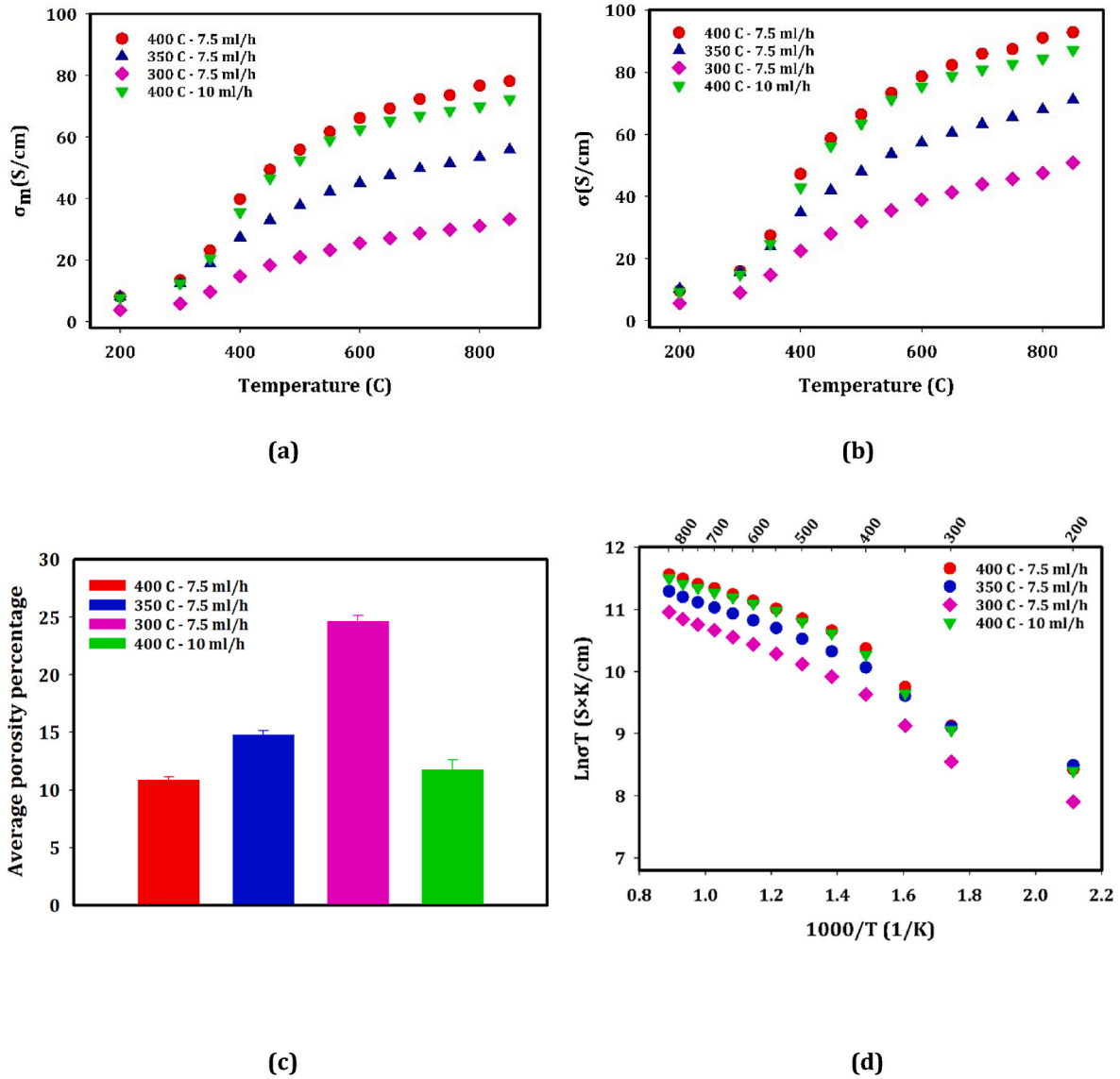

Fig. 11. (a) Measured electrical conductivity of the deposited spinel oxide coatings at the different temperatures and spraying speeds, (b) electrical conductivity of the deposited spinel oxide coatings at the different temperatures and spraying speeds modified with the average porosity percentage, (c) the measured average porosity percentage of the deposited spinel oxide coatings at the different temperatures and spraying speeds, and (d) Arrhenius diagram presenting the correlation between electrical conductivity and applied temperature during Van Der Pauw measurement for the deposited spinel oxide coatings.

deposited spinel oxide coatings at different temperatures with different spraying speeds. Arrhenius diagrams correlate the electrical conductivity of spinel oxide coatings with applied temperature during Van Der Pauw measurement. The activation energy needed for electrical conductivity could be calculated for each sample according to Eq. (7):

$$\mathrm{Ln}\sigma T = \frac{-E_a}{kT} + \mathrm{Ln}\ \sigma_0 \quad (7)$$

In this equation, E_a (eV/K) is the activation energy, T (K) is the temperature, σ (S/cm) is the electrical conductivity, σ_0 is the pre-exponential factor and K is the Boltzmann's constant which is equal to 8.617×10^{-5} eV/K. The values of the activation energy and pre-exponential factors calculated for two temperature ranges including 300–400 °C and 450–850 °C, are reported in Table 3. At the higher temperatures, mobility of the charge carriers inside crystal lattice of Fe modified Mn_2CuO_4 spinel oxide increases, which facilitates their movement and decrease the needed energy to transfer charge [71,72].

Moreover, the results show that the activation energy of the deposited spinel oxide coatings reduces with increasing deposition temperature. It means that in the spinel oxide coatings with more uniform and dense structure, mobility of the charge carriers inside the crystal lattice is easier than in spinel oxide coatings with cracks and pores. Indeed, uniform and dense microstructure without cracks can facilitate the

Table 3
The values of the calculated activation energy and pre-exponential factor for the deposited spinel oxide coatings at the different temperatures with different spraying speeds.

Deposition temperature (°C)	Spraying speed (ml/h)	Temperature range	E_a (eV)	Ln σ_0
400	7.5	300–400	0.42	17.47
		850–450	0.16	13.17
350	7.5	300–400	0.31	15.54
		850–450	0.18	12.98
300	7.5	300–400	0.38	19.18
		850–450	0.2	12.77
400	10	300–400	0.43	17.19
		850–450	0.17	13.05

movement of charge species. The needed activation energies for the mobility of the charge transfer species for the spinel oxide coating deposited are 0.2 eV and 0.16 eV for deposited coatings at 300 °C and 400 °C (with the same spraying speed), respectively. Our findings agree with other researchers' reported activation energy for Mn_2CuO_4 spinel oxide materials [74,75]. However, increasing spraying speed for the deposited spinel oxide coatings at 400 °C has negligible effect on the electrical conductivity and the needed activation energy.

Our obtained results are in good agreement with other researches. For example, for $Mn_{1.7}CuFe_{0.3}O_4$ powders (pellets) synthesized with sol-gel method, the electrical conductivity value at 800 °C is reported 69 S/cm [38]. Also, for $Cu_{1.15}Mn_{1.55}Fe_{0.3}O_4$ synthesized with sol-gel and solid-state reaction methods, the electrical conductivity value at 800 °C are reported around 106 and 12 S/cm, respectively [17]. Up to now, there was no available data for $Mn_{1.5}CuFe_{1.5}O_4$ spinel oxide materials in the form of coating or powder. Our measured value for electrical conductivity of $Mn_{1.5}CuFe_{1.5}O_4$ spinel oxide coatings at 800 °C is 78.12 S/cm (before correction with porosity), which is above required value (> 50 S/cm) in the temperature range of 400–850 °C.

4. Conclusions

In the present research, the spray pyrolysis method as a simple, accessible and cost-effective method was used to prepare Fe-modified Mn_2CuO_4 spinel oxide coatings on the surface of Crofer 22 APU metallic interconnect and alumina. Obtained results suggest that the spray pyrolysis method could be a promising method for preparing dense and thick spinel oxide coatings with uniform, defect-free and not-cracked microstructure. The main conclusions based on our results are drawn and listed below.

1. Increasing deposition temperatures from 250 °C up to 400 °C, resulted in reducing and elimination of cracks, voids and defects, and achieving dense and uniform layer.
2. Increasing spraying speed to more than 10 ml/h led to increasing cracks, voids and delamination on the surface of spinel oxide coatings.
3. Deposition temperature influenced the crystallization of the spinel oxide coatings during the deposition process.
4. The deposited spinel oxide coating on alumina was pure cubic spinel oxide, and Crofer 22 APU was a mixture of cubic and tetragonal spinel oxides. No impurities were observed in X-ray pattern.
5. Prepared spinel oxide coatings at higher deposition temperatures with lower spraying speed showed lower average roughness.
6. The deposited spinel oxide coatings at the higher deposition temperature with lower spraying speeds showed higher electrical conductivity.
7. Increasing deposition temperature reduced the activation energy for charge transfer throughout the spinel oxide coatings. While, increasing spraying speed showed a negligible effect on the activation energy.

CRediT authorship contribution statement

Maryam Mehdizade: Writing – original draft, Visualization, Validation, Software, Methodology, Investigation, Formal analysis, Data curation, Conceptualization. **Federico Smeacetto:** Writing – review & editing, Visualization, Validation, Data curation, Conceptualization. **Michał Winiarski:** Writing – review & editing, Formal analysis, Data curation. **Sebastian Molin:** Writing – review & editing, Validation, Supervision, Resources, Project administration, Funding acquisition, Data curation, Conceptualization.

Declaration of competing interest

The authors declare that they have no known competing financial interests or personal relationships that could have appeared to influence the work reported in this paper.

Acknowledgments

This research supported by National Science Centre (NCN) Opus project number 2023/49/B/ST8/03265: Alternative to alloying: advanced protective coatings for low-cost alloys for solid oxide cell stack technology.

Appendix A. Supplementary data

Supplementary data to this article can be found online at https://doi.org/10.1016/j.ijhydene.2025.04.355.

References

[1] Zhu H, Zhang J, Cao W. Recent advances in spinel-based protective coatings produced by electrochemical method on metallic interconnects for solid oxide fuel cells. Int J Hydrogen Energy 2024;50:977–91. https://doi.org/10.1016/j.ijhydene.2023.09.242.
[2] Mahato N, Banerjee A, Gupta A, Omar S, Balani K. Progress in material selection for solid oxide fuel cell technology: a review. Prog Mater Sci 2015;72:141–337. https://doi.org/10.1016/j.pmatsci.2015.01.001.
[3] Shaheen N, Chen Z, Nong Y, Su T, Yousaf M, Alomar M, Lu Y. Progress in nano-technology development and nano-material selection for low-temperature solid oxide fuel cell. J Alloys Compd 2024;977:173212. https://doi.org/10.1016/j.jallcom.2023.173212.
[4] Li J, Zhang Y, Zhao K, Jiang SP, Chen M. An investigation of Cr vaporization from SUS430 metallic interconnect and deposition on (La,Sr)MnO3 cathode of intermediate temperature solid oxide fuel cells. J Power Sources 2023;579:233285. https://doi.org/10.1016/j.jpowsour.2023.233285.
[5] Geng S, Zhao Q, Li Y, Mu J, Chen G, Wang F, Zhu S. Sputtered MnCu metallic coating on ferritic stainless steel for solid oxide fuel cell interconnects application. Int J Hydrogen Energy 2017;42:10298–307. https://doi.org/10.1016/j.ijhydene.2017.01.178.
[6] Zhou L, Li W, Brady MP, Eldred TB, Garcia R, Ma L, Wang Y, Hu S, Li W, Liu X. Long-term oxidation and chromium evaporation behavior of Al2O3-forming austenitic stainless steel for 900 °C balance-of-plant components applications in solid oxide fuel cells. Int J Hydrogen Energy 2024;50:1109–25. https://doi.org/10.1016/j.ijhydene.2023.10.041.
[7] Eikeng E, Makhsoos A, Pollet BG. Critical and strategic raw materials for electrolysers, fuel cells, metal hydrides and hydrogen separation technologies. Int J Hydrogen Energy 2024;71:433–64. https://doi.org/10.1016/j.ijhydene.2024.05.096.
[8] Kim TH, Song RH, Mehran MT, Joh DW, Hussain A, Lee SB, Lim TH, Hong JE. Effects of Mn concentration on durability of Fe-Cr ferritic steels dispersed with La2O3 for solid oxide fuel cell interconnects. J Power Sources 2024;594:234020. https://doi.org/10.1016/j.jpowsour.2023.234020.
[9] Mao J, Wang E, Wang H, Ouyang M, Chen Y, Hu H, Lu L, Ren D, Liu Y. Progress in metal corrosion mechanism and protective coating technology for interconnect and metal support of solid oxide cells. Renew Sustain Energy Rev 2023;185. https://doi.org/10.1016/j.rser.2023.113597.
[10] Li F, Zhang P, Zhao Y, Yang D, Sun J. The preparation and properties of Mn–Co–O spinel coating for SOFC metallic interconnect. Int J Hydrogen Energy 2023;48:16048–56. https://doi.org/10.1016/j.ijhydene.2023.01.065.
[11] Talic B, Falk-Windisch H, Venkatachalam V, Hendriksen PV, Wiik K, Lein HL. Effect of coating density on oxidation resistance and Cr vaporization from solid oxide fuel cell interconnects. J Power Sources 2017;354:57–67. https://doi.org/10.1016/j.jpowsour.2017.04.023.
[12] Reddy MJ, Kamecki B, Talic B, Zanchi E, Smeacetto F, Hardy JS, Choi JP, Mazur L, Vasßen R, Basu SN, Brylewski T, Svensson JE, Froitzheim J. Experimental review of the performances of protective coatings for interconnects in solid oxide fuel cells. J Power Sources 2023;568. https://doi.org/10.1016/j.jpowsour.2023.232831.
[13] Hassan MA, Bin Mamat O, Mehdi M. Review: influence of alloy addition and spinel coatings on Cr-based metallic interconnects of solid oxide fuel cells. Int J Hydrogen Energy 2020;45:25191–209. https://doi.org/10.1016/j.ijhydene.2020.06.234.
[14] Zhu Z, Darl-Uzu C, Pal U, Gopalan S, Hussain AM, Dale N, Fukuyama Y, Miura Y, Miyoshi Y, Basu S. Comparison of Cu–Mn and Mn–Co spinel coatings for solid oxide fuel cell interconnects. Int J Hydrogen Energy 2022;47:36953–63. https://doi.org/10.1016/j.ijhydene.2022.08.239.
[15] Gao J, Si X, Wang X, Li C, Qi J, Cao J. Exploring the effects of Mn content in the Mn-Co spinel coating on its formation and slowing the outward Cr diffusion. Corros Sci 2023;217:111158. https://doi.org/10.1016/j.corsci.2023.111158.
[16] Ekhlasiosgouei O, Smeacetto F, Molin S. Suspension and process parameters selection for electrophoretic deposition of Mn–Co spinel coating on steel interconnects. Int J Hydrogen Energy 2024;60:1054–67. https://doi.org/10.1016/j.ijhydene.2024.02.252.
[17] Mazur Ł, Koszelow D, Zajusz M, Łapiński M, Bik M, Zając P, Adamczyk A, Rutkowski P, Molin S, Brylewski T. Comparison of Cu1.3Mn1.7O4 spinels doped with Ni or Fe and synthesized via wet chemistry and solid-state reaction methods,

designed as potential coating materials for metallic interconnects. J Eur Ceram Soc 2023;43:5557–74. https://doi.org/10.1016/j.jeurceramsoc.2023.05.015.
[18] Ranjbar-Nouri Z, Soltanieh M, Rastegari S. Applying the protective CuMn2O4 spinel coating on AISI-430 ferritic stainless steel used as solid oxide fuel cell interconnects. Surf Coating Technol 2018;334:365–72. https://doi.org/10.1016/j.surfcoat.2017.11.036.
[19] Mazur L, Domaradzki K, Winiarski P, Zych L, Brylewski T. Optimization of electrophoretic deposition and thermal treatment of Cu–Mn spinel matrix for spinel/perovskite composite coating used as SOC metallic interconnect. Ceram Int 2024;50:34017–26. https://doi.org/10.1016/j.ceramint.2024.06.221.
[20] Acharya N, Chaitra U, Vijeth H, Sagar R. Highly dense Mn3O4 and CuMn2O4 spinels as efficient protective coatings on solid oxide fuel cell interconnect and their chromium diffusion studies. J Alloys Compd 2022;918:165377. https://doi.org/10.1016/j.jallcom.2022.165377.
[21] Ekhlasiosgouei O, Bik M, Molin S. Preparation of MnCo2O4 and Mn1.7CuFe0.3O4 single-layer, and novel MnCo2O4/Mn1.7CuFe0.3O4 dual-layer spinel protective coatings on complex-shaped metallic interconnects by EPD method. Int J Hydrogen Energy 2024;83:563–76. https://doi.org/10.1016/j.ijhydene.2024.07.447.
[22] Wang J, Chen W, Hu X, Zhou J, Chen B, Zhang Z, Jiang L, Jiang X. Effect of Fe on the oxidation behavior, electrical properties and microstructure of Co–Ni protective coatings for metal interconnect layers in solid oxide fuel cells. Mater Char 2024;211:113899. https://doi.org/10.1016/j.matchar.2024.113899.
[23] Zhou J, Hu X, Li J, Jiang X. Cu doped Ni–Co spinel protective coatings for solid oxide fuel cell interconnects application. Int J Hydrogen Energy 2021;46:33580–93. https://doi.org/10.1016/j.ijhydene.2021.07.173.
[24] Zhao M, Geng S, Chen G, Wang F. Thermal conversion and evolution behavior of surface scale on SOFC interconnect steel with sputtered FeCoNi coating. Corros Sci 2020;168:108561. https://doi.org/10.1016/j.corsci.2020.108561.
[25] Zhu H, Geng S, Chen G, Wang F. Electrophoretic deposition of trimanganese tetraoxide coatings on Ni-coated SUS 430 steel interconnect. J Alloys Compd 2019;782:100–9. https://doi.org/10.1016/j.jallcom.2018.12.174.
[26] Geng S, Pan Y, Chen G, Wang F. CuFe 2 O 4 protective and electrically conductive coating thermally converted from sputtered CuFe alloy layer on SUS 430 stainless steel interconnect. Int J Hydrogen Energy 2019;44:9400–7. https://doi.org/10.1016/j.ijhydene.2019.02.117.
[27] Liu D, Geng S, Chen G, Wang F. The performance of NiO/NiFe2O4 coated pre-oxidized SUS 430 interconnect with different NiO thickness for solid oxide fuel cell. Ceram Int 2024;50:25749–62. https://doi.org/10.1016/j.ceramint.2024.04.311.
[28] Sabato AG, Molin S, Javed H, Zanchi E, Boccaccini AR, Smeacetto F. In-situ Cu-doped MnCo-spinel coatings for solid oxide cell interconnects processed by electrophoretic deposition. Ceram Int 2019;45:19148–57. https://doi.org/10.1016/j.ceramint.2019.06.161.
[29] Tan KH, Rahman HA, Taib H. Coating layer and influence of transition metal for ferritic stainless steel interconnector solid oxide fuel cell: a review. Int J Hydrogen Energy 2019;44:30591–605. https://doi.org/10.1016/j.ijhydene.2019.06.155.
[30] Talic B, Molin S, Wiik K, Hendriksen PV, Lein HL. Comparison of iron and copper doped manganese cobalt spinel oxides as protective coatings for solid oxide fuel cell interconnects. J Power Sources 2017;372:145–56. https://doi.org/10.1016/j.jpowsour.2017.10.060.
[31] Qiao W-QQ, Li Y-WW, Zhang Y-SS, Wang M-HH, Li K, Li Z-JJ, Yang W. Cu- and Ce-doped MnCo2O4 spinel coatings on ferrite interconnects by electrophoretic deposition. Mater Today Commun 2024;38:108061. https://doi.org/10.1016/j.mtcomm.2024.108061.
[32] Zanchi E, Molin S, Sabato AG, Talic B, Cempura G, Boccaccini AR, Smeacetto F. Iron doped manganese cobaltite spinel coatings produced by electrophoretic co-deposition on interconnects for solid oxide cells: microstructural and electrical characterization. J Power Sources 2020;455. https://doi.org/10.1016/j.jpowsour.2020.227910.
[33] Du L, Li J, Liao Q, Qin N, Bao D. Ce-doping at Mn site to enhance resistive switching performance of spinel MnCo2O4 resistive random access memory devices. Ceram Int 2024;50:20495–503. https://doi.org/10.1016/j.ceramint.2024.03.171.
[34] Zhang YY, Zhang YY, Wu C, Yang Y, Li Q, Chen Y. Oxidation behavior and electrical properties of metal interconnects with Ce-doped Ni–Mn spinel coatings. Ceram Int 2022;48:9550–7. https://doi.org/10.1016/j.ceramint.2021.12.153.
[35] Wang B, Li K, Liu J, Zhang T, Yang T, Zhang N. Promoting electric conductivity of MnCo spinel coating by doping transition metals (Cu, Fe) or rare-earth elements (La, Y) for solid oxide fuel cell interconnect. Int J Hydrogen Energy 2024;61:216–25. https://doi.org/10.1016/j.ijhydene.2024.02.198.
[36] Lemieszek B, Ignaczak J, Lankauf K, Błaszczak P, Bik M, Zając M, Sitarz M, Jasiński P, Molin S. CuMn1.7Fe0.3O4 – RE2O3 (RE = Y, Gd) bilayers as protective interconnect coatings for solid oxide cells. J Eur Ceram Soc 2024;44. https://doi.org/10.1016/j.jeurceramsoc.2024.116743.
[37] Safikhani A, Esmailian M, Tinatiseresht T, Darband GB. High temperature cyclic oxidation behavior of ferritic stainless steel with addition of alloying elements Nb and Ti for use in SOFCs interconnect. Int J Hydrogen Energy 2016;41:6045–52. https://doi.org/10.1016/j.ijhydene.2016.01.090.
[38] Ignaczak J, Zeng L, Sanchez DF, Makowska M, Górnicka K, Lankauf K, Karczewski J, Jasiński P, Molin S. Fe-modified Mn2CuO4 spinel oxides: coatings based on abundant elements for solid oxide cell interconnects. Int J Hydrogen Energy 2023;48:36076–93. https://doi.org/10.1016/j.ijhydene.2023.06.041.
[39] Brylewski T, Kruk A, Bobruk M, Adamczyk A, Partyka J, Rutkowski P. Structure and electrical properties of Cu-doped Mn-Co-O spinel prepared via soft chemistry and its application in intermediate-temperature solid oxide fuel cell interconnects. J Power Sources 2016;333:145–55. https://doi.org/10.1016/j.jpowsour.2016.09.136.
[40] Saeidpour F, Ebrahimifar H. Effect of nanostructure Fe-Ni-Co spinel oxides/Y2O3 coatings on the high-temperature oxidation behavior of Crofer 22 APU stainless steel interconnect. Corros Sci 2021;182:109280. https://doi.org/10.1016/j.corsci.2021.109280.
[41] Kamecki B, Karczewski J, Miruszewski T, Jasiński G, Szymczewska D, Jasiński P, Molin S. Low temperature deposition of dense MnCo2O4 protective coatings for steel interconnects of solid oxide cells. J Eur Ceram Soc 2018;38:4576–9. https://doi.org/10.1016/j.jeurceramsoc.2018.05.042.
[42] Kamecki B, Karczewski J, Jasiński P, Molin S. Improvement of oxygen electrode performance of intermediate temperature solid oxide cells by spray pyrolysis deposited active layers. Adv Mater Interfac 2021;8:1–11. https://doi.org/10.1002/admi.202002227.
[43] Montero X, Tietz F, Sebold D, Buchkremer HP, Ringuede A, Cassir M, Laresgoiti A, Villarreal I. MnCo1.9Fe0.1O4 spinel protection layer on commercial ferritic steels for interconnect applications in solid oxide fuel cells. J Power Sources 2008;184:172–9. https://doi.org/10.1016/j.jpowsour.2008.05.081.
[44] Tian Y, Wang H, Liu S, Zhang B. Synthesis, optimization, electrochemical and electrochromic properties of Zr-doped NiO films by chemical spray pyrolysis. Electrochim Acta 2024;506:145057. https://doi.org/10.1016/j.electacta.2024.145057.
[45] Stoermer AO, Rupp JLM, Gauckler LJ. Spray pyrolysis of electrolyte interlayers for vacuum plasma-sprayed SOFC. Solid State Ionics 2006;177:2075–9. https://doi.org/10.1016/j.ssi.2006.06.033.
[46] Bik M, Stygar M, Jeleń P, Dąbrowa J, Leśniak M, Brylewski T, Sitarz M. Protective-conducting coatings based on black glasses (SiOC) for application in Solid Oxide Fuel Cells. Int J Hydrogen Energy 2017;42:27298–307. https://doi.org/10.1016/j.ijhydene.2017.09.069.
[47] Jalilvand G, Faghihi-Sani MA. Fe doped Ni-Co spinel protective coating on ferritic stainless steel for SOFC interconnect application. Int J Hydrogen Energy 2013;38:12007–14. https://doi.org/10.1016/j.ijhydene.2013.06.105.
[48] Zhao Q, Geng S, Chen G, Wang F. Comparison of electroplating and sputtering Ni for Ni/NiFe2 dual layer coating on ferritic stainless steel interconnect. Corros Sci 2021;192:109837. https://doi.org/10.1016/j.corsci.2021.109837.
[49] Johnson C, Orlovskaya N, Coratolo A, Cross C, Wu J, Gemmen R, Liu X. The effect of coating crystallization and substrate impurities on magnetron sputtered doped LaCrO3 coatings for metallic solid oxide fuel cell interconnects. Int J Hydrogen Energy 2009;34:2408–15. https://doi.org/10.1016/j.ijhydene.2008.12.072.
[50] Cavichiolo LS, Nørby TH, Hald J, Pantleon K. Long-term effects of soft-chromising Ni-electroplated AISI 441 commodity steel for SOC stack interconnects. Corros Sci 2024;227. https://doi.org/10.1016/j.corsci.2023.111728.
[51] Wolff M, Schwiers A, Wilkner K, Sebold D, Menzler NH. Wet powder spraying – a versatile and highly effective technique for the application of spinel-type protective coatings on SOC interconnects. J Power Sources 2024;592. https://doi.org/10.1016/j.jpowsour.2023.233931.
[52] Hu YZ, Yun LL, Wei T, Li CX, Qi Z, Yang GJ, Li CJ, Liu M. Aerosol sprayed Mn1.5Co1.5O4 protective coatings for metallic interconnect of solid oxide fuel cells. Int J Hydrogen Energy 2016;41:20305–13. https://doi.org/10.1016/j.ijhydene.2016.09.096.
[53] Sun Z, Wang R, Nikiforov AY, Gopalan S, Pal UB, Basu SN. CuMn1.8O4 protective coatings on metallic interconnects for prevention of Cr-poisoning in solid oxide fuel cells. J Power Sources 2018;378:125–33. https://doi.org/10.1016/j.jpowsour.2017.12.031.
[54] dos Santos-Gómez L, Zamudio-García J, Porras-Vázquez JM, Losilla ER, Marrero-López D. Recent progress in nanostructured electrodes for solid oxide fuel cells deposited by spray pyrolysis. J Power Sources 2021;507. https://doi.org/10.1016/j.jpowsour.2021.230277.
[55] Kamecki B, Karczewski J, Cempura G, Jasiński P, Molin S. Evaluation of structural and electrical properties of multicomponent spinel oxide thin films deposited via spray pyrolysis technique. Mater Char 2023;203. https://doi.org/10.1016/j.matchar.2023.113097. 0–5.
[56] Doubi Y, Hartiti B, Labrim H, Tahri M, Laazizi A, Thevenin P. Elaboration of spinel Co3O4 via cost-effective chemical spray pyrolysis for enhanced photo-response. Mater Today Commun 2024;40:110207. https://doi.org/10.1016/j.mtcomm.2024.110207.
[57] Kate RS, Pathan HM, Kalubarme R, Kale BB, Deokate RJ. Spray pyrolysis: approaches for nanostructured metal oxide films in energy storage application. J Energy Storage 2022;54:105387. https://doi.org/10.1016/j.est.2022.105387.
[58] Ryll T, Reibisch P, Schlagenhauf L, Bieberle-Huetter A, Döbeli M, Rupp JLM, Gauckler LJ. Lanthanum nickelate thin films deposited by spray pyrolysis: crystallization, microstructure and electrochemical properties. J Eur Ceram Soc 2012;32:1701–9. https://doi.org/10.1016/j.jeurceramsoc.2011.12.032.
[59] Rupp JLMM, Scherrer B, Harvey AS, Gauckler LJ. Crystallization and grain growth kinetics for precipitation-based ceramics: a case study on amorphous ceria thin films from spray pyrolysis. Adv Funct Mater 2009;19:2790–9. https://doi.org/10.1002/adfm.200900255.
[60] Simons P, Torres KP, Rupp JLM. Deposition parameters and Raman crystal orientation measurements of ceria thin films deposited by spray pyrolysis. J Mater Chem 2022;A:8898–910. https://doi.org/10.1039/d1ta09115h.
[61] Kamecki B, Cempura G, Jasiński P, Wang SF, Molin S. Tuning electrochemical performance by microstructural optimization of the nanocrystalline functional oxygen electrode layer for solid oxide cells. ACS Appl Mater Interfaces 2022;14:57449–59. https://doi.org/10.1021/acsami.2c18951.
[62] Radić N, Stojadinović S, Ilić M, Kasalica K, Tsanev A. Eu-doped ZnO coatings prepared by spray pyrolysis for photocatalytic applications. Inorg Chem Commun 2024;167. https://doi.org/10.1016/j.inoche.2024.112822.

[63] Kurichenko VL, Argunov EV, Karpenkov DY, Kolesnikov EA. Investigation of nanostructured FeNi hollow microspheres properties synthesized by ultrasonic spray pyrolysis. Adv Powder Technol 2024;35:104461. https://doi.org/10.1016/j.apt.2024.104461.
[64] Kinonshita T, Murakami D, Wada Y, Okada Y. Synthesis of nickel–cerium oxide solid-solution hollow fine particles by ultrasonic spray pyrolysis with citric acid addition. Adv Powder Technol 2024;35. https://doi.org/10.1016/j.apt.2024.104563.
[65] Perednis D, Gauckler LJ. Solid oxide fuel cells with electrolytes prepared via spray pyrolysis. Solid State Ionics 2004;166:229–39. https://doi.org/10.1016/j.ssi.2003.11.011.
[66] Perednis D, Wilhelm O, Pratsinis SE, Gauckler LJ. Morphology and deposition of thin yttria-stabilized zirconia films using spray pyrolysis. Thin Solid Films 2005;474:84–95. https://doi.org/10.1016/j.tsf.2004.08.014.
[67] Beckel D, Dubach A, Studart AR, Gauckler LJ. Spray pyrolysis of La0.6Sr0.4Co0.2Fe0.8O3-δ thin film cathodes. J Electroceram 2006;16:221–8. https://doi.org/10.1007/s10832-006-6971-3.
[68] Perednis D, Gauckler LJ. Thin film deposition using spray pyrolysis. J Electroceram 2005;14:103–11. https://doi.org/10.1007/s10832-005-0870-x.
[69] Sheikhzadeh M, Sanjabi S. Coelectrodeposition of crystalline copper-manganese oxide containing CuMn2O4 spinel for high energy supercapacitor application. Synth Met 2021;278:116802. https://doi.org/10.1016/j.synthmet.2021.116802.
[70] Adamczyk A, Bik M, Kruk A, Pyzalski M, Brylewski T. Crystallization and decomposition of Mn1.5Co1.5O4 spinel synthesized using EDTA gel processing. J Therm Anal Calorim 2024;149:2561–72. https://doi.org/10.1007/s10973-023-12839-1.
[71] Gillot B, Kharroubi M, Metz R, Legros R, Rousset A. Electrical properties of copper manganite spinels CuxMn3−xO4 (0 > x > 1). Phys Status Solidi 1991;124:317–25. https://doi.org/10.1002/pssa.2211240130.
[72] Petric A, Ling H. Electrical conductivity and thermal expansion of spinels at elevated temperatures. J Am Ceram Soc 2007;90:1515–20. https://doi.org/10.1111/j.1551-2916.2007.01522.x.
[73] Ponpandian N, Balaya P, Narayanasamy A. Electrical conductivity and dielectric behaviour of nanocrystalline NiFe2O4 spinel. J Phys Condens Matter 2002;14:3221–37. https://doi.org/10.1088/0953-8984/14/12/311.
[74] Waluyo NS, Park BK, Lee SB, Lim TH, Park SJ, Song RH, Lee JW. Mn,Cu)3O4-based conductive coatings as effective barriers to high-temperature oxidation of metallic interconnects for solid oxide fuel cells. J Solid State Electrochem 2014;18:445–52. https://doi.org/10.1007/s10008-013-2245-6.
[75] Ignaczak J, Naumovich Y, Górnicka K, Jamroz J, Wróbel W, Karczewski J, Chen M, Jasiński P, Molin S. Preparation and characterisation of iron substituted Mn1.7Cu1.3-xFexO4 spinel oxides (x = 0, 0.1, 0.3, 0.5). J Eur Ceram Soc 2020;40:5920–9. https://doi.org/10.1016/j.jeurceramsoc.2020.07.001.